Journal of Electroceramics, 6, 169–207, 2001

Review: Deposition of Ceramic Thin Films at Low Temperatures from Aqueous Solutions

THOMAS P. NIESEN[1] & MARK R. DE GUIRE[2]

[1]*Max-Planck-Institut für Metallforschung and Institut für Nichtmetallische Anorganische Materialien, Universität Stuttgart, Pulvermetallurgisches Laboratorium, Heisenbergstraße 5, D-70569 Stuttgart, Germany**

[2]*Department of Materials Science & Engineering, Case Western Reserve University, 10900 Euclid Avenue, Cleveland, Ohio 44106-7204, USA*

Submitted February 16, 2000; Revised January 3, 2001; Accepted January 3, 2001

Abstract. Many techniques for the synthesis of ceramic thin films from aqueous solutions at low temperatures (25–100°C) have been reported. This paper reviews non-electrochemical, non-hydrothermal, low-temperature aqueous deposition routes, with an emphasis on oxide materials for electronic applications. Originally used for sulfide and selenide thin films, such techniques have also been applied to oxides since the 1970's. Films of single oxides (e.g., transition metal oxides, In_2O_3, SiO_2, SnO_2) and multicomponent films (doped ZnO, Cd_2SnO_4, $ZrTiO_4$, ZrO_2-Y_2O_3, Li-Co-O spinel, ferrites, perovskites) have been produced. The maximum thicknesses of the films obtained have ranged from 100 to 1000 nm, and deposition rates have ranged from 2 to 20,000 nm/h. Compared to vapor-deposition techniques, liquid-deposition routes offer lower capital equipment costs, lower processing temperatures, and flexibility in the choice of substrates with respect to topography and thermal stability. Compared to sol-gel techniques, the routes reviewed here offer lower processing temperatures, lower shrinkage, and (being based on aqueous precursors) lower costs and the potential for reduced environmental impact. This review emphasizes the influence of solution chemistry and process design on the microstructures and growth rates of the films. The current understanding of the mechanisms of film formation is presented, and the advantages and limitations of these techniques are discussed.

Keywords: thin films, ceramic, synthesis, liquid phase deposition, chemical bath deposition

1. Introduction

Techniques for the synthesis of ceramic[1] thin films from aqueous solutions at low temperatures are emerging as possible alternatives to vapor-phase [1, 2] and chemical-precursor [3, 4] techniques. Lower temperatures allow films to be deposited on substrates that might not be chemically or mechanically stable at high temperatures. Unlike vapor-phase processes, techniques that use liquids as the deposition medium do not rely on line-of-sight deposition, so that non-planar substrates can be coated. The equipment for liquid-based techniques is simple and much less costly than, e.g., vacuum systems and glove boxes. Finally, with aqueous solutions and readily available reagents, there is reduced reliance on expensive or sensitive organometallic precursors and the potential for reduced environmental impact, in comparison with many chemical routes. (Single-crystalline films can be obtained via either aqueous or organic routes, as recently reviewed by Lange [5], but all require a thermal decomposition step at temperatures usually between 150 and 500°C.)

On the other hand, the chemical versatility of sol-gel and polymer-pyrolysis routes has enabled them to be utilized to synthesize virtually any ceramic material of technological interest. Vapor phase techniques, after more than two decades of widespread research, are well known to offer a high level of control over the composition, microstructure, and growth rates of the resulting films. Aqueous deposition techniques for ceramic films have not yet reached this level of development. Nevertheless, their potential to produce ceramic films over large areas at comparatively low cost has

*Current address: Siemens & Shell Solar GmbH, Otto-Hahn-Ring, D-81739 München, Germany.

continued to make these techniques attractive and has stimulated a resurgence of interest in them since the mid 1980's.

The main techniques for the non-electrochemical synthesis of polycrystalline ceramic films from aqueous solutions at low temperatures, and some of the materials produced using them, are listed below:

- Chemical bath deposition (CBD)—CoO [6], Co_3O_4 [7], NiO [8–10], AgO [11], Ag_2O [11], ZnO [12–17], CdO [12, 18, 19], In_2O_3 [20], SnO_2 [21], Cd_2SnO_4 [13]; CdS, ZnS, Sn_xS, PbS, MnS, CoS, NiS, Cu_xS, Ag_2S, As_2S_3, Sb_2S_3, Bi_2S_3, MoS_2, and corresponding selenides (see reviews in Refs. [22–25])
- Successive ion layer adsorption and reaction (SILAR)—MnO_2 [26], $FeOOH/Fe_2O_3$ [27], NiO [28], Cu_2O [29, 30], CuO [31], ZnO [32–39] and ZnO with Ni, Cu, or Cd doping [40], Tl_2O_3 [41], SnO_2 [42], $LaNbO_x$ [43], CeO_{2+x} [44] and Y, La and Eu hydroperoxide [45]; ZnS [46, 47], CdS [46, 48, 49], PbS [50], CoS [51], CuS [52, 53], Ag_2S [54], Sb_2S_3 [55, 56], In_2S_3 [57] and Bi_2Se_3 [58].
- Liquid phase deposition (LPD)—SiO_2 (see review in Ref. [59]), TiO_2 [60–66], ZrO_2 [67], V_2O_5 [68, 69], β-FeOOH/α-Fe_2O_3 [70], $NiFe_2O_4$ [62], $LnMO_3$ (Ln = La, Nd; M = Cr, Mn, Fe, Co) [71, 72], SnO_2 [73]
- Electroless deposition (ED) with catalyst (Ag^+, Sn^{2+}, or Pd^{2+})—MnO_2 [74], $La_{1-x}MnO_3$ [75], ZnO [76, 77], In_2O_3 [78], Tl_2O_3 [74], α-PbO_2 [79]

These main techniques are reviewed here, as well as significant variations, including: photochemical deposition (PCD), deposition assisted by applied fields, ferrite plating, use of functionalized surfaces, and liquid flow deposition (LFD). Additional materials and developments are being reported monthly, from research groups in every part of the world. While each of the techniques reviewed here is distinct, all use aqueous solutions at low temperatures ($<100^\circ$C) to yield polycrystalline or amorphous films. In some of the literature covered here, extensions beyond our present scope will be mentioned briefly, e.g., non-aqueous solutions, more complex structures, and non-electronic applications.

2. Main Techniques

2.1. Chemical Bath Deposition (CBD)

2.1.1. Introductory remarks. Of all the deposition techniques described here, chemical bath deposition of metal chalcogenide films is by far the oldest. To the best of our knowledge, it dates to 1884, when PbS thin films were first deposited in the presence of thiourea ($SC(NH_2)_2$) [80]. The term "chemical bath deposition" is recent; we adopt it here as the generic name for techniques that produce a solid film in a single immersion through control of the kinetics of formation of the solid, typically without changing the metals' oxidation state.[2] In recent decades, many sulfides and selenides have been prepared by this technique. This work has been summarized in several reviews [22–25, 81]. The number of materials is expanded by the ability to synthesize ternary phases (or doped films) either by codeposition [22] or by interdiffusion of previously deposited multilayers [82, 83].

Although the CBD literature is dominated by work on sulfide and selenide thin films, this technique has been used for the deposition of oxide thin films, with potential for large-area applications in semiconductor devices. The work on oxides (reviewed later in this paper) is relatively new. Therefore, the range of oxides that has been produced is much narrower, and the understanding of processing-property relationships is less advanced, than is the case with sulfide and selenide films. The next section (§ 2.1.2) describes CBD in terms applicable to both oxide and non-oxide films. That is followed by a review of research on the mechanism of deposition of CdS films (§ 2.1.3), which provides insights into the mechanism of CBD in general (§ 2.1.4). Then CBD of oxide films is reviewed (§ 2.1.5), followed by a discussion of the applications of films (non-oxide and oxide) deposited via CBD (§ 2.1.6).

2.1.2. General description. The deposition medium for CBD consists of one or more salts of metal M^{n+}, a source for the chalcogenide X (X = O, S, Se), and usually a complexing agent, in aqueous solution. Typically, the metal salts are chosen for their moderate to high solubility in water, e.g., chlorides, nitrates, sulfates, or acetates. Examples of chalcogenide sources include thiourea, thiosulfate ($S_2O_3^{2-}$), or thioacetamide (CH_3CSNH_2) for S^{2-} ions and selenourea ($SeC(NH_2)_2$) or selenosulfate ($SSeO_3^{2-}$) for Se^{2-} ions, while the water itself provides oxygen in the form of OH^- ions. The complexing agent provides ligands such as ammonia (NH_3), triethanolamine ($N(CH_2CH_2OH)_3$), citrate ($[HOC(COO)(CH_2COO)_2]^{3-}$), tartrate ($[OOC(CHOH)_2COO]^{2-}$), cyanide ($CN^-$) or ethylenediamine ($H_2N(CH_2)_2NH_2$).

The processes that occur in the CBD solution consist in general of the following steps:

1) Equilibrium between the complexing agent and water;
2) Formation/dissociation of ionic metal-ligand complexes $[M(L)_i]^{n-ik}$, where L^{k-} denotes one or more ligands;
3) Hydrolysis of the chalcogenide source;
4) Formation of the solid.

Most of the control that can be exerted over the film growth process resides in adjustment of the last three steps. Hydrolysis of the chalcogenide source (step 3) is critical because it provides the desired non-metal species that pull the metal cations out of solution to form the solid film. The kinetics of this step are highly sensitive to the solution's pH and temperature, as well as to the catalytic effects of certain solid species that may be present. In principle, the formation of the solid M_mX_n (step 4) begins when the rising concentration of X^{m-} from step 3 causes the ionic product $[M^{n+}]^m[X^{m-}]^n$ to exceed the solubility product. In practice, the central issue is whether the solid forms as a film or as particles dispersed in the liquid; and in the case of film formation, whether deposition proceeds by ion-by-ion growth on the substrate (i.e., by successive cation and anion adsorption) or by a colloidal or cluster mechanism (i.e., by adsorption and coagulation of colloids that were formed in the solution). Lastly, the formation of complexed metal ions (step 2) allows control over the rate of formation of solid metal hydroxides,[3] which competes with step 4 and which would otherwise occur immediately in the normally alkaline solutions. These steps together determine the composition, growth rate, microstructure, and topography of the resulting thin films. Therefore, they are the focal point for efforts to control the films' properties and their suitability for applications.

2.1.3. Deposition mechanism of CdS by CBD. Within the framework of the four main reaction steps listed in § 2.1.2, the deposition of CdS in aqueous ammonia from thiourea and a cadmium salt can be formulated as:

NH_3-H_2O equilibrium:

$$2NH_3 + 2H_2O \Leftrightarrow 2NH_4^+ + 2OH^- \qquad (1)$$

dissociation of Cd complex:

$$Cd(NH_3)_4^{2+} \Leftrightarrow Cd^{2+}(aq) + 4NH_3(aq) \qquad (2)$$

hydrolysis of thiourea:

$$S{=}C(NH_2)_2 + 2OH^- \rightarrow S^{2-}(aq) + H_2NC{\equiv}N + 2H_2O \qquad (3)$$

formation of CdS:

$$Cd^{2+}(aq) + S^{2-}(aq) \rightarrow CdS(s) \qquad (4)$$

net reaction:

$$Cd(NH_3)_4^{2+} + S{=}C(NH_2)_2 \rightarrow CdS(s) + H_2NC{\equiv}N + 2NH_4^+ + 2NH_3 \qquad (5)$$

In this sequence, ammonia controls the concentrations of both S^{2-} (by providing OH^- ions for the hydrolysis of thiourea) and free Cd^{2+} ions (by providing NH_3 for complexation).

The formation of thin CdS films by CBD dates to 1961, when Mokrushin and Tkachev [84] added NaOH to accelerate the decomposition of thiourea at room temperature and deposited films on a variety of substrates, including glass, porcelain, plexiglass and quartz. The authors differentiated two types of film growth and suggested that a primary compact and mirrorlike layer was formed by small colloidal particles (i.e., by cluster growth). A secondary layer of larger, agglomerated particles was loosely attached to the first layer.

Based on these observations and assumptions, Kitaev et al. [85–91] gained the first key insights into the mechanism of film formation. They established via a radiochemical technique that colloidal $Cd(OH)_2$ particles are able to adsorb and to decompose thiourea molecules to initiate the formation of CdS [92, 93]. The forming chalcogenide itself, like the hydroxide nuclei, also catalyzes the thiourea decomposition. That is, the process, once started, is autocatalytic, and a hydroxide phase is only necessary for activation. Regarding the catalytic process as a necessary first step to forming CdS films, they used a simple thermodynamic equilibrium analysis to define conditions for forming the hydroxide. Assuming a starting solution with cadmium concentration $[Cd] = 10^{-3}$ M and a thiourea concentration of 10^{-2} M (Fig. 1), cadmium hydroxide will be stable at pH values above the "hydroxide line," whereas the complex ion $Cd(NH_3)_4^{2+}$ will exist only below the "complex line." Therefore, to form $Cd(OH)_2$, it is necessary either to use an ammonia concentration

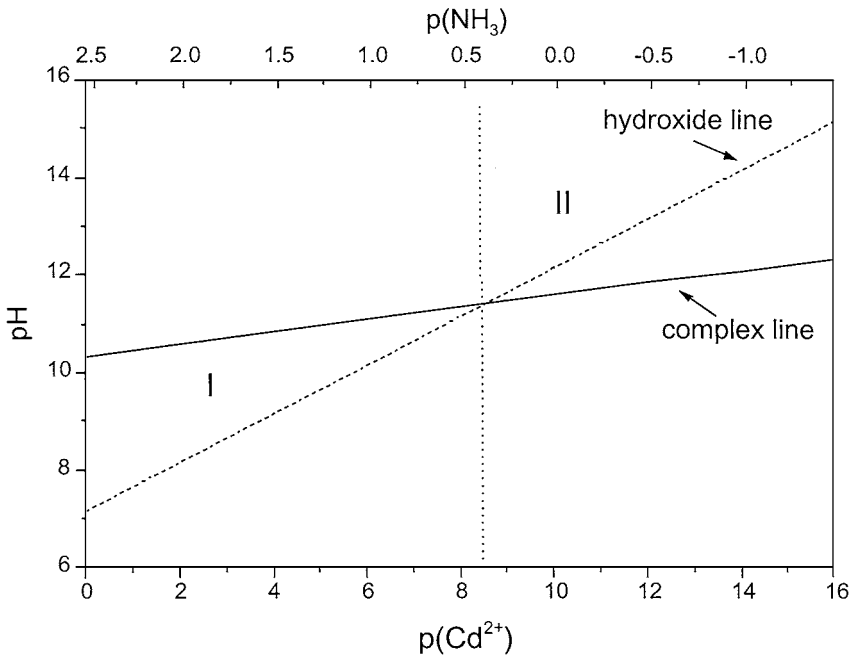

Fig. 1. Graphical solution of the thermodymic equilibrium analysis calculated for a cadmium salt concentration of 10^{-3} M. The calculation includes the equilibra $Cd(OH)_2 = Cd^{2+} + 2OH^-$ and $Cd(NH_3)^{2+} = Cd^{2+} + 4NH_3$. Cadmium hydroxide will only be formed in region I (inevitably) or II (by adding alkali). Adapted from ref. [86].

$[NH_3]$ <0.4 M (region I) or to add, e.g., 1–4 $\times$ 10^{-2} M alkali (region II).

Later results of Pavaskar et al. [94] and Chopra et al. [95] corroborate their analysis. Raising the temperature to 80–90°C under such conditions led likewise to adherent films while clear solutions (i.e., containing no $Cd(OH)_2$ precipitates) yielded less adherent and powdery films. The authors proposed that clear solutions could undergo slow thermal hydrolysis of thiourea and subsequent formation of powdery films of colloidal CdS. In contrast, the proper solution chemistry seems to lead to early $Cd(OH)_2$ formation on the substrate, leading to the formation of adherent films of predominantly hexagonal CdS. Rieke and Bentjen [96] were indeed able to show that adherent and specularly reflecting CdS films could only be formed in a pH range [9.0 < pH < 10.4] for which a $Cd(OH)_2$ film formed on the substrate's surface. Results on CdSe films showed many similarities [97].

These later results strongly support an ion-by-ion growth mechanism based on the surface-catalyzed thiourea decomposition. Therefore, Lincot and Ortega-Borges [98, 99] proposed the following reaction steps:

1. Reversible adsorption of cadmium hydroxide species:

$$Cd(NH_3)_4^{2+} + 2OH^- + \text{site} \Leftrightarrow [Cd(OH)_2]_{ads} + 4NH_3 \quad (6)$$

2. Formation of a surface complex with thiourea:

$$[Cd(OH)_2]_{ads} + S{=}C(NH_2)_2 \rightarrow [Cd(S{=}C(NH_2)_2)(OH)_2]^*_{ads} \quad (7)$$

3. Formation of CdS with site regeneration:

$$[(Cd(S{=}C(NH_2)_2)(OH)_2]^*_{ads} \rightarrow CdS(s) + H_2NC{\equiv}N + 2H_2O + \text{site} \quad (8)$$

(Note that the net reaction of this sequence,

$$Cd(NH_3)_4^{2+} + S{=}C(NH_2)_2 + 2OH^- \rightarrow CdS(s) + H_2NC{\equiv}N + 2H_2O + 4NH_3 \quad (9)$$

when combined with the ammonia-water equilibrium (Eq. (1)), yields a net reaction that is identical to

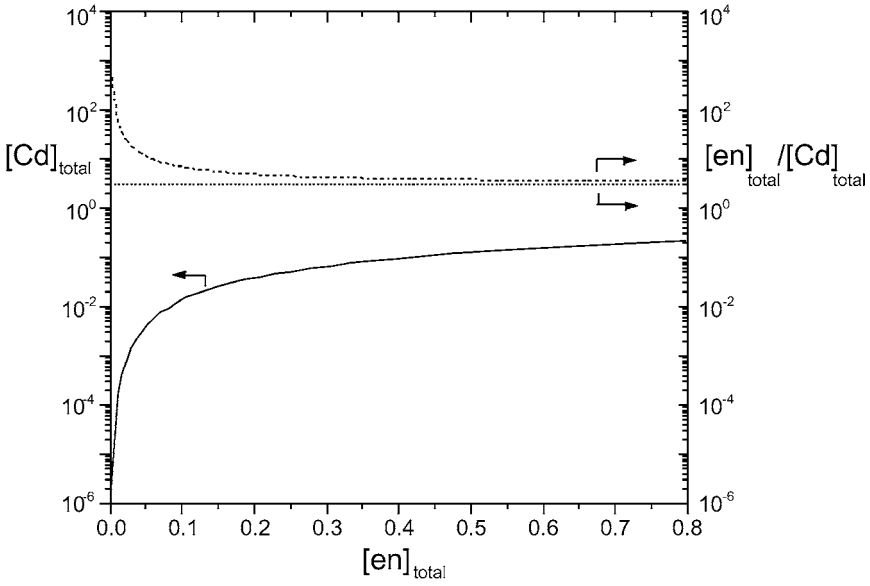

Fig. 2. Equivalent solution contour plot for $pCd^{2+} = 9$ at 50°C (straight line) and its concentration dependent ratio $[en]_{total}/[Cd]_{total}$ (dashed line) compared to a constant ratio (doted line). Adapted from ref. [103].

Eq. (5)). In this mechanism, the rate-determining step is reaction (8), the decomposition of the metastable complex formed in reaction (7). Doña and Herrero [100, 101] proposed a slightly different intermediate species, $[Cd(OH)_2(NH_3)_2]_{ads}$, taking into account the tendency of transition metal ions to form mixed aqueous-ammonia complexes and the higher $[OH^-]/[NH_3]$ ratio at the substrate surface compared to the solution.

Lincot and Ortega-Borges [98, 99] also investigated the kinetics of deposition of CdS films. Under conditions of $[Cd^{2+}] = 4$–30 mM, [thiourea] = 28 mM, $[NH_3] = 1.74$ M, and $T = 60$°C, compact, adherent films grew up to 0.1–0.2 μm thick, consisting of well-defined hexagonal crystallites, tens of nanometers in size. Initially, the growth rate was low while the pH rose and nucleation took place on the surface. Then the growth rate increased to a constant value (e.g., to 300 nm/h for $[Cd^{2+}] = 4$ mM and 900 nm/h for $[Cd^{2+}] = 30$ mM). Growth beyond this linear stage occurred at a higher rate, as much smaller (3–6 nm) mixed hexagonal/cubic crystallites deposited from the solution to form a porous outer layer.

From the previous discussion it is obvious that the predominance of the ion-by-ion growth mode is limited to certain bath compositions and is strongly dependent on the elapsed deposition time. Gorer and Hodes [102], using potassium nitrilotriacetate (NTA) as a chelating agent during growth of CdSe films, noticed a change in the deposition mechanism at a critical value of $[NTA]/[Cd^{2+}]$. O'Brien and McAleese [103] expanded this concept towards an "equivalent solution contour plot", i.e., a plot of total ligand concentration against total metal ion concentration at a constant value of free metal ions (Fig. 2). Such plots are based on the assumption that the concentration $[Cd^{2+}(aq)]$ of *free* metal ions is more important than the concentrations of complexed, precipitated, or total metal ions for maintaining good quality film deposition. They take into account that much higher values of $[en]/[Cd]_{tot}$ are needed to maintain an empirically determined [104], optimal value of $[Cd^{2+}(aq)]$ at low $[Cd]_{tot}$, due to the tendency of complexes to dissociate on dilution. "Critical ratios" of $[en]/[Cd]_{tot}$ could be defined for each value of $[Cd]_{tot}$ or, as a limiting case, at high concentrations. Below such a critical ratio R_c, Gorer and Hodes postulated that a hydroxide mechanism prevails: a visible precipitate of $Cd(OH)_2$ forms and is adsorbed on the substrate, and subsequent growth occurs from diffusion of colloidal particles (CdSe or $Cd(OH)_2$) to the surface. It was suggested that growth occurs from attachment of single crystals or aggregates with surface energies high enough to promote the adherence to the growing film. Above R_c, ion-by-ion growth was assumed. The authors suggested that after a single molecule of

CdSe is on the substrate, it might grow by additional adsorption of Cd^{2+} and Se^{2-} species to form larger clusters (i.e., cluster formation on-site). This was recently experimentally shown by Breen et al. [105] who investigated CdS deposition on freshly cleaved mica using atomic force microscopy. They detected the formation of island-like CdS deposits in the first 3 min, each deposit 0.4–0.6 nm in height and 10–40 nm across. The islands (or clusters on-site) seem to grow out from the substrate rather than along its surface, competing with the formation of new islands on the mica surface for Cd and S. In other words, no initial formation of a featureless coating was observed during the early growth stages of ion-by ion growth.

Although typical CBD processes for non-oxide films use basic conditions, modestly *acidic* baths would minimize the problem of bulk hydroxide formation. Lokhande [106] was first able to form CdS films from a thiosulfate-containing bath. In acidic medium, the thiosulfate dissociates into hydrogen sulfite (HSO_3^-) and sulfur, which is reduced by the thiosulfate itself to sulfide ions. Recently, O'Brien and co-workers [107] reported on the deposition of CdS thin films from cadmium chloride, thioacetamide and urea. The thin films are polycrystalline, constisting of large particles (hexagonal CdS, ca. 300–500 nm in diameter) which are composed of smaller grains, ca. 10–20 nm in diameter. So far, no details about the mechanism of film formation under acidic conditions were reported.

2.1.4. Conclusions: mechanism of film growth via CBD. Two parameters seem to have major influence on the deposition of thin films by CBD: 1) the choice of complexant and its concentration (relative to the cation concentration employed), by determining the free metal cation concentration; and 2) the pH of the solution, by offering the possibility of hydroxide formation and by its connection with the decomposition of the chalcogenide source, either directly or indirectly. Both parameters determine the available free [M] and [chalcogenide] for the metal chalcogenide formation, i.e., the degree to which the solubility limit is exceeded.

Kitaev's assertion that the formation of $Cd(OH)_2$ is necessary to initiate the growth of high-quality CdS film via CBD appears to be correct; the best films are formed under conditions that thermodynamically favor the formation of $Cd(OH)_2$. The critical issue is *where* the $Cd(OH)_2$ forms. Once the solid phase is nucleated, the same solution conditions and fundamental mechanisms that lead to ion-by-ion growth of a film can also lead to the growth of primary colloidal particles in the solution.

If $Cd(OH)_2$ forms on the substrate, ion-by-ion growth of CdS via a surface-catalyzed decomposition of the chalcogenide-delivering species can occur. If the concentration of complexants is sufficiently high to suppress the bulk precipitation of the hydroxide, while still permitting its formation on the substrate, growth can occur solely via ion-by-ion growth. Such conditions are desirable because they afford the greatest control over the growth process, but they are very difficult to reach and maintain in a liquid solution. In gas-phase deposition methods, in contrast, the substrate can be heated (or a plasma can be located near the substrate), which favors the occurrence of the reaction on the substrate only. Furthermore, in CVD processes the reactants flow continuously through the chamber, making it easier to maintain concentrations at constant values. These differences may promote atom-by-atom growth in CVD, making it the prevalent process of growth for high-quality CVD films. Conversely, modifying CBD techniques so as to confine the reactions as much as possible to the substrate and to flow the reactants past the substrate (see § 3.3 and § 3.5.) may afford greater control over the mode of growth of films in CBD.

Several authors noticed a highly oriented nature of the films perpendicular to the substrate [101, 108, 109], and if InP single crystals are used as substrates (and [complexant]/[Cd] $> R_c$), epitaxial growth of hexagonal CdS or cubic CdSe was possible [110–112]. Orientation of the films seems to be a distinctive characteristic of ion-by-ion growth mode.

If $Cd(OH)_2$ particles appear in the solution, nucleation and growth of CdS particles in the bulk will compete with any growth of solid at the surface. These particles, if they are small enough, may form (or contribute to the growth of) a dense film. However, the window of time during which such growth can occur is limited, because the same forces that cause particles to attach to a growing film of the same solid will simultaneously cause them to tend to agglomerate with each other. Such agglomerates can form powdery, nonadherent films, or porous outer layers on dense films.

For compounds that can exist in more than one crystalline form, the appearance of a particular polymorph does not permit unambiguous determination of the mechanism of film growth. HRTEM investigations of CdS films by Froment and Lincot [111] showed that stacking faults are responsible for changes in growth habit from hexagonal to cubic. The density of these

defects is highly dependent upon the deposition conditions, which could explain why different polymorphs were reported in the literature. Gibson et al. [113] postulated a polytype CdS structure, consisting of nearly random stacking sequences of the hexagonal planes that form the basis for cubic and hexagonal modification. Their Rietveld simulation showed all the main features seen in many reported experimental patterns even when no hexagonal- or cubic-like sequences appear in the model structure.

In conclusion, both mechanisms for film growth (ion-by-ion growth, or particle attachment) can produce dense, adherent, mirror-like films. Because similar solution conditions permit either mechanism to take place, they can occur simultaneously, or ion-by-ion growth can be succeeded by particle attachment. Transparency of the deposition medium does not rule out the possibility of growth by particle attachment: clear solutions may contain sub-visible particles (smaller than the wavelength of light) that could participate in film growth. According to Gorer and Hodes, the two mechanisms yield characteristic crystal sizes: approx. 5 nm below R_c (attachment of particles) and approx. 16 nm above R_c (ion-by-ion growth). Comparable results were reported by Lincot and co-workers [108, 109].

Nair et al. [114] incorporated these considerations into a simple mathematical model for predicting the rate of chalcogenide film growth. The model is based on the simplifying assumption that the decomposition of the metal complex (e.g., Eq. (2)), rather than any of the intermediate steps considered by Lincot and Ortega-Borges [98, 99] or Doña and Herrero [100, 101] limits the growth rate. Therefore, first-order reaction kinetics are expected. Growth is assumed to occur in ion-by-ion mode. Precipitation kinetics are included in the model as a sink for reactants and not as a mode of film growth. The model gives only qualitative agreement with significant empirical observations. In particular, thin films are obtained from dilute solutions at high temperatures (a thermally forced reaction, running quickly to completion), while thicker films require concentrated solutions and lower temperatures. Kostoglou et al. [115] derived a much more detailed mathematical model based on the deposition mechanism proposed by Doña and Herrero [100, 101], capable of quantitatively explaining the experimentally observed behavior. For example, the experimentally and theoretically derived film growth rates with time at different temperatures are in striking agreement. Therefore, this model offers for the first time the potential to optimize the CBD process without experimental work. While the complete model is rather complicated and has to be numerically solved, a simplified version was derived, which is in qualitative agreement with the experimental results.

2.1.5. CBD of oxide films. In broad outline, the four main reaction steps given in § 2.1.2 apply as well to CBD of oxide films. In those cases where a complexing agent is used, step 1 (the equilibrium between water and the complexing agent) is the same for non-oxide and oxide depositions, and the role of the ligand remains one of slowing down the rate of solid formation. The analogous process to step 3, hydrolysis of the chalcogenide source, is essentially the dissociation reaction of water. Step 2, the association/dissociation equilibrium of the solvated metal complex, can be thought of as being replaced by a process in which the ligands of the complex are displaced by hydroxyl groups to form a solid hydroxide compound. Step 4, the formation of the desired product, can come about via deprotonation of the hydroxide compound to form the oxide. (In several cases described below, the hydroxide was converted to the oxide only after heating the as-deposited film at 150–400°C.)

For a metal cation M^{n+} complexed by i ligands L^{k-}, these last three steps can be formulated as the following reactions:

dissociation of water:

$$n\mathrm{H_2O} \Leftrightarrow n\mathrm{OH^-} + n\mathrm{H^+} \tag{10}$$

displacement of ligands:

$$n\mathrm{OH^-} + \mathrm{M(L)}_i^{(n-ik)+} \rightarrow \mathrm{M(OH)}_n(\mathrm{s}) + i\ \mathrm{L}^{k-} \tag{11}$$

deprotonation to form oxide:

$$\mathrm{M(OH)}_n(\mathrm{s}) \rightarrow \mathrm{MO}_{n/2}(\mathrm{s}) + n/2\mathrm{H_2O} \tag{12}$$

net reaction:

$$\mathrm{M(L)}_i^{(n-ik)+} + n/2\mathrm{H_2O} \rightarrow \mathrm{MO}_{n/2}(\mathrm{s}) + n\mathrm{H^+} + i\mathrm{L}^{k-} \tag{13}$$

The hydrolytic process depicted by reactions (11) and (12) is sometimes called "forced hydrolysis" [116]. It does not require addition of base, even though the hydroxyl ion appears on the left side of (11). It can be accelerated simply by heating the solution, which induces deprotonation of the hydrated metal species. (Not coincidentally, the effects of adding base or raising

the temperature here parallel those described by Kitaev for CdS formation, discussed in § 2.1.3.) Hydrolysis can occur even in acidic solutions when the metal cation is easily hydrolyzable, as with Fe^{3+}, Ti^{4+}, Zr^{4+}, Al^{3+}.

The similarities between Eqs. (5) or (9) and (13) are clear: a solvated metal complex reacts with a chalcogenide source to form a desired solid product. The main difference is that, for the non-oxide films discussed so far, the chalcogenide source is present in a dilute concentration (typically 0.01–0.1 M). This concentration constitutes an additional parameter that, along with pH and temperature, permits control to be exerted over the rate of decomposition of the chalcogenide source. In CBD of oxides, the "chalcogenide source" is water, the medium of deposition. Thus tighter control would have to be exerted over just two parameters (pH, T) to achieve a similar degree of control over the rate of hydrolysis (and, by implication, control over the film's microstructure and properties). (In some cases, as will be explained below, a way around this limitation has been the use of hydrogen peroxide or potassium persulfate as oxidizing agents, leading first to a film-forming non-stochiometric superoxide).

Table 1 lists oxides that have been deposited in thin-film form via CBD and summarizes the deposition parameters, maximum thicknesses, and growth rates. The first such report was in 1980 by Call et al. [12], who inadvertently produced ZnO and CdO while attempting to deposit mixed (Cd, Zn)S films via CBD. They then optimized their conditions to obtain adherent, single-phase, crystalline ZnO (hexagonal, partial {100} orientation) and CdO (cubic, rocksalt structure) films. For example, cadmium-containing films were deposited from a solution containing cyanide (as a complexant) and hydrogen peroxide (as an oxidizing agent) at 80°C. They were transformed to cubic CdO (rock salt structure) by heat treatment at 250–300°C. Single immersions gave films up to 200 nm thick; repetitions of this process led to thicknesses greater than 1 μm. Later Najdoski et al. [18] showed that $Cd(O_2)_{0.88}(OH)_{0.24}$ films are formed initially in such cases. In contrast, Ocampo et al. [19] formed first $Cd(OH)_2$ films from aqueous ammonia solutions at 50°C, followed by subsequent thermal annealing to CdO at 400°C.

After the early work on ZnO films by Call et al. [12], Varkey [16] and O'Brien et al. [14, 15] deposited randomly oriented hexagonal ZnO films. O'Brien et al. showed that simple thermodynamic calculations (using published solubility products and dissociation constants) accurately predicted the ranges of pH and ligand/metal ratio over which solid would form at 50°C. Obtaining adherent, uniform films required still narrower ranges of these parameters. That is, thermodynamics could predict precipitation, but was insufficient to predict whether a film would form and, if so, what its morphology would be.

The hexagonal ZnO films deposited by Ennaoui et al. [17] exhibited preferred {002} orientation but also contained $Zn(OH)_2$ as revealed by XPS. Considering the mechanism of deposition, they concluded that their adherent, hard, and specularly reflecting ZnO films grew heterogeneously via adsorption of zinc complexes on the substrate followed by reaction to form the solid, while thicker, powdery, and less adherent films formed via sedimentation of particles formed in the solution.

The formation of other transition-metal oxide films using CBD has been reported. Pramanik and Bhattacharya [8] synthesized NiO films from a solution of nickel sulfate, potassium persulfate (oxidizer), and ammonia (complexant) at room temperature. The authors suggested that an intermediate nickel superoxide is formed that is subsequently reduced by ammonia. Varkey and Fort formed NiO films from nickel sulfate solution by forced hydrolysis [9]. The highest growth rates reported so far for NiO film deposition (680 nm h^{-1}, Table 1) were recently reached by Pejova et al. [10] using a solution of nickel nitrate and urea at ~100°C. The as-deposited nickel hydroxide films were transformed to NiO by air annealing at 350–400°C. CoOOH (converted to Co_3O_4 on heating above 300°C) [7] and AgO [11] films have been prepared by oxidation of the lower-valent metal ions during forced hydrolysis. Eze [6] synthesized hydrated CoO films from solutions of $CoCl_2$, NH_3, and NaOH, which converted to the crystalline oxide (CoO) on heating to 300–400°C. Nanocrystalline SnO_2, and an amorphous yttrium basic carbonate precursor to Y_2O_3, were deposited on oxidized silicon substrates using forced hydrolysis; this work is discussed in more detail in § 3.4.

Raviendra and co-workers synthesized undoped and doped ZnO and In_2O_3, [13, 20] SnO_2, [21] and Cd_2SnO_4 [13] films as transparent semiconductors for optical and electronic applications. They used chlorides as metal sources, NH_4F (which they called a "freezing agent") as a complexant, and $AgNO_3$ as a "catalyst". The $AgNO_3$ undoubtedly resulted in AgCl colloid formation, though its occurrence and role were not discussed. Their films crystallized after post-deposition heat treatments; no crystallinity of their films prior to heat treatment was reported.

Table 1. Oxide thin films deposited via chemical bath deposition (CBD).

System		Complexant/ pH control	Temperature (°C)			pH	Growth rate (nm h^{-1})	Max. thickness (nm)	Reference
Oxide	Substrate		Deposition	As-deposited	Annealing				
Y_2O_3	SiO_2/Si	Urea	80	Amorphous Y basic carbonate	600	4–6.5	~2	35	[274]
CoOOH, Co_3O_4	Glass	NH_3	65–70	CoOOH	≥300 (Co_3O_4)	12	25	100	[7]
CoO	Glass	NH_3	25–60	$CoO{\cdot}6H_2O$	300–400 (CoO)	11–12	24–108	120–680 (1×) 1,300 (2×)	[6]
NiO	Glass	NH_3	25	Polycrystalline	n.r.	Basic	275	275	[8]
NiO, NiOOH	Glass	NH_3	57–77	NiO	280 (NiOOH)	Basic	~60	120	[9]
NiO	Glass	Urea	~100	$3Ni(OH)_2{\cdot}2H_2O$	350–400	6.0	680	900	[10]
AgO, Ag_2O	Glass	TEA[a]	25	AgO	≥150 (Ag_2O)	>11.5	10–20	100	[11]
ZnO	Glass	KCN	80–90	Polycrystalline	350	Basic	n.r.	400 (1×) 1,500 (2×)	[12]
ZnO, ZnO:Al	Glass, SiO_2 glass	NH_3	25	$Zn(OH)_2$	180–450	7.5–8.5	2,600–4,800	870	[13]
ZnO	Glass	en[b], TEA[a]	65	Hydrated oxide	250	Basic	2,200–3,300	40,000	[16]
ZnO	Glass, SnO_2 on glass	en[b]	50	Polycrystalline	None	10.5–11	n.r.	n.r.	[14, 15]
ZnO	Glass, $CuInS_2$	NH_3	65	ZnO, $Zn(OH)_2$	≥200	7.5–13.7	≥40	n.r.	[17]
CdO	Glass	KCN	80	Polycrystalline	250–300	Basic	n.r.	200 (1×) >1,000 (>2×)	[12]
CdO	Glass, SiO_2	NH_3	20–25	$Cd(O_2)_{0.88}(OH)_{0.24}$	195	10	100–175	800	[18]
CdO	Glass	NH_3	50	$Cd(OH)_2$	≥300	Basic	n.r.	n.r.	[19]
In_2O_3, In_2O_3:Sn	Glass, SiO_2 glass, Al_2O_3, Si	NH_3	25	Hydrated oxide	200	7.5–8.5	1,200	360	[20]
SnO_2	SiO_2/Si	None	80	Cassiterite	None	1.3–1.5	3–10	50 (1×) 82 (2×)	[270–272]
SnO_2, SnO_2:Sb	Glass, SiO_2 glass	NH_3	25	Amorphous	170	7.5–8.5	1,400–2,300	850	[21]
Cd_2SnO_4	Glass, SiO_2 glass	NH_3	25	Amorphous	>200	7.5–8.5	1,200–2,100	720	[13]

[a]TEA = triethanolamine.
[b]en = ethylene diamine.

Raviendra et al. described their process as "controlled homogeneous precipitation" (note the probable formation of AgCl colloids) and asserted that formation of the solid only need occur *near* the substrate (not necessarily in contact with it) to result in growth of a film. The process was self-limiting, ceasing when the product of ionic concentrations dropped below the solubility product. They attributed this drop in concentration to depletion of reactants at low pH, and to bulk precipitation at high pH. Up to that point, their films grew at constant rates of 20–80 nm min^{-1} (the higher values occurring at higher pH) to thicknesses of 400–800 nm (the higher values occurring at lower pH). This phenomenon has since been observed by others (see ref. [117, 118] for example). When the degree of supersaturation is increased by changing (here, raising) the pH (or, in the case of sulfides, raising the thiourea concentration), the initial growth rate is raised, but the limiting thickness is reduced. Solutions that are less heavily supersaturated grow more slowly but ultimately provide thicker films—a "tortoise and hare" effect. These observations are consistent with Nair's model [114] regarding the effects of metal concentrations and temperature (see above). Overall, the growth rate is determined by supersaturation (temperature and pH), while thickness is limited by the supply of reactants (starting concentrations and—if ion-by-ion growth dominates—avoidance of precipitation).

2.1.6. Applications. Among the first trial applications for CBD thin chalogenide films were PbSe photoconductive cells [119] in 1949 and PbS photodiodes in the mid 1960's [120, 121]. Although the promising photosensitive properties of the films were recognized, their implementation did not progress beyond laboratory devices.

Nair [122, 123] drew attention to the advantages of chemically deposited thin films for use in solar cell applications. In a solar cell, charge carriers are optically generated at a p-n junction. Heterojunction solar cells, in which the junction is formed between two different polycrystalline compound semiconductors, are potentially much cheaper and more efficient than cells based on single-crystal silicon [124, 125]. During the past twenty years, two heterojunction systems with potential module efficiencies >10% have been intensively investigated: cadmium telluride/cadmium sulfide (p-CdTe/n-CdS) and copper indium diselenide/cadmium sulfide (p-$CuInSe_2$/n-CdS). In both cases, a thin CdS layer fulfills the dual role of forming the heterojunction and of acting as a transparent window. CBD CdS thin films are suffiently thin (50–100 nm) to allow the required high transmission and sufficiently continuous to avoid any short circuits. Today, both BP Solar and Siemens Solar use CBD to produce the CdS component of the *Apollo* series solar cells (CdTe/CdS) [126] or the *ST series* thin film modules (CIS technology) [127] respectively.

The necessary n-type conductivity can be achieved in CBD CdS thin films either by thermal annealing in air at 400–500°C or by ion exchange reaction followed by thermal annealing at 200°C [128]. The thermal treatment leads to the formation of a top CdO layer which is highly n-type due to incomplete oxidation. Ion-exchange leads to n-type or p-type conductivity, by Hg^+ or Cu^+ exchange, respectively. For a CdS film, electrical conductivity increased nine orders of magnitude under illumination to 10 Ω^{-1} cm^{-1}, the highest values of sensitivity and photoconductivity reported so far for any physical or chemical deposition method. In 1991, Chu et al. [129, 130] first used CBD CdS thin films 60–100 nm thick for the fabrication of n-CdS/p-CdTe solar cells. Boron doping was used to reduce the resistivity of the CdS film and an efficiency higher than 14.5% was reported.

In case of the $CuInSe_2$-based cells, resistivity losses are best minimized by use of an additional transparent and current-collecting ZnO layer on top of the CdS thin film [124]. Early devices achieved a conversion efficiency of 11% [131]. A buffer layer < 100 nm thick is used to maximize the optical transmission. For this layer, CBD offers the advantage of a shift of the absorption edge to shorter wavelength, arising from quantum size effects in semiconductors with particle sizes between 1 and 5 nm. Recently, $Cu(In, Ga)Se_2$/CBD-CdS/ZnO solar cells with an efficiency up to 17% have been fabricated [132]. Other research groups successfully replaced the toxic CdS by CBD-grown $In_x(OH, S)_y$, $Zn(S, OH)_x$ or $Zn(Se, OH)_x$ [133–140].

The efficiency of $CuInSe_2$/CdS thin film solar cells in which both layers were produced by CBD was relatively low (<3%) [141]. This was attributed to high sheet resistance of the CdS layer, high carrier concentration in the absorber layer and/or low grain size of the $CuInSe_2$ film.

Several groups have sought an explanation for the high efficiency of CBD-based solar cells. The main nitrogen impurity in as-deposited films is probably cyanamide (NCN^{2-}), arising from thiourea

decomposition (see Eq. (5)). Oxygen is incorporated in the form of water, hydroxide or carbonate [96, 142–145]. Weber et al. [146] detected up to 12 atom-% hydrogen in the films and assumed that additional hydrogen in form of HS^- ions is abundant at the grain boundaries. Nakada and Kunioka [147, 148] found that Cd diffuses into Cu(In, Ga)Se_2 during CBD of the CdS overlayer and replaces Cu to a depth of ∼10 nm, leading to a buried *np*-junction at the interface. Kronik et al. [149] have shown that the CdS buffer layer restores interface surface charge on CIGS, due to creation of Cd_{Cu} interface donors and possibly removal of O_{Se} interface acceptors. Similar interdiffusion processes were reported for the CdS/CdTe interface [150, 151]. By secondary ion mass spectroscopy, Boyle et al. [152] detected maxima in the ^{12}C, ^{34}S and ^{35}Cl isotopic profiles located at the CdS-CdTe interface after thermal annealing and a high ^{16}O concentration throughout the cell structure. It appears that both impurities and the excess Cd indeed play an important role in the efficiency of the CBD-derived cells, but that properties deteriorate when impurity levels exceed an upper limit [145].

Nair and co-workers demonstrated further prospective applications for CBD films related to solar energy. Cu_xS thin films were used as solar control coatings [153, 154], which allow a controlled amount of natural light to enter a building but which reject as much infrared radiation as possible. Multiple films, e.g., SnS-CuS, PbS-CuS and Bi_2S_3-CuS, were likewise proven to be useful as solar absorber coatings [24]. Finally, a metal sulfide thin film photography (MSTF) based on photoaccelerated chemical deposition (PACD) was tested. PACD takes advantage of a higher deposition rate (due to an increase of the bath temperature by photothermal conversion of incident radiation) and a higher condensation rate (due to the presence of photogenerated charge carriers). The resulting differences in Bi_2S_3 film thickness led to tone variations of the optical interference colors and resulted in photographic imaging [155].

Oxide films deposited via CBD, while apparently not having reached commercial application yet, have been proposed for use in wavelength-selective (UV- or IR-reflective, or antireflective) multilayer coatings on glass for architectural applications [6, 9, 15], as insulating or semiconducting layers in solar-cell structures [9, 11, 17, 19], as transparent conductors [14, 15, 19], as electrochromic thin films [9], and as low-emittance coatings [16].

2.2. *SILAR*

2.2.1. Introductory remarks. The successive ionic-layer absorption and reaction (SILAR) process was developed for the deposition of sulfide thin films by Nicolau [46] in the mid 80's as a liquid-phase counterpart of gas-phase atomic layer epitaxy. Independently, Ristov et al. [29] reported a comparable technique for the deposition of oxide thin films. The distinguishing characteristic of SILAR techniques is the use of alternating aqueous solutions (a metal salt solution, followed by a hydrolyzing or sulfidizing solution). In principle, this is intended to allow ion-by-ion growth of the compound film via sequential addition of individual atomic layers. The advantages of automating this process were recognized at an early stage: in his first paper, Nicolau presented a computer-driven deposition apparatus that consists of beakers for the solutions and rinsing vessels lying in a circle [46, 156]. Early work on SILAR was summarized by Tolstoi in 1993 [157].

The next section (§ 2.2.2) describes the formation of sulfide thin films by SILAR, followed by a description of the mechanism of film formation (§ 2.2.3). Then oxide thin films deposited by the SILAR technique (§ 2.2.4) and applications of SILAR films (§ 2.2.5) are summarized.

2.2.2. SILAR of sulfide thin films. Strongly adherent CdS, ZnS and $Zn_{1-x}Cd_xS$ thin films were formed on single crystal and polycrystalline substrates at room temperature by Nicolau and co-workers [158]. The authors used slightly acidic solutions of the uncomplexed cation (from sulfate or chloride, 0.005–5 M) and alkaline sodium sulfide solutions (0.005–2.8 M), i.e., the film-forming species were present in much higher concentration than in the CBD technique. Both solutions were kept at ambient temperature but under inert atmosphere to prevent oxidation of the sulfide. On indium-tin oxide (ITO)-coated glass, polycrystalline CdS (hexagonal) thin films were formed with mean crystallite sizes of 30 nm (perpendicular to the film) and 15 nm (parallel), and a strong ⟨0001⟩ orientation (columnar structure). Likewise, polycrystalline cubic ZnS thin films were grown with a mean crystallite size of 6.5 nm (perpendicular to the substrate) and 4 nm (parallel to the substrate) and a weak ⟨111⟩ orientation. Growth rates were about 1.3 Å per cycle, which is typical for the SILAR technique. Lindroos et al. [47, 159] deposited adherent ZnS thin films on various polymer substrates. Films on poly(vinyl chloride) and

polycarbonate were polycrystalline. In contrast, films on polyester substrates were amorphous but showed polycrystallinity when the film thickness exceeded 250 nm.

$Zn_{1-x}Cd_xS$ thin films obtained using mixed Zn and Cd salt solutions or sequentially applied single-cation sources were true ZnS-CdS solid solutions [158, 160, 161]. Likewise, doping of ZnS thin films with Mn was achieved either by separate immersions into a manganese salt solution or by use of mixed salt solutions [158, 162, 163]. Multilayers of ZnS and CdS for potential application in light-emitting devices have been grown on ITO-covered glass [48, 49]. The individual layers were up to 50 nm thick and no diffusion of the cations from layer to layer could be detected.

SILAR is even able to promote epitaxial growth at room temperature, a fact that was related to the high surface diffusion coefficients of the adsorbed ions and the long surface diffusion time available to reach the lattice kinks. On single-crystal InP and GaAs substrates, (hetero) epitaxial hexagonal CdS and cubic ZnS thin films were grown, up to 300 nm in thickness. To obtain similar structures, gas-phase deposition processes have to be operated at temperatures several hundreds of degrees higher [158].

A combination of the CBD and SILAR techniques involves the use of complexed ions as the cation precursor, a technique first used by Kanniainen et al. [50] to deposit cubic PbS thin films. By island-like growth [164, 165], crystallites grew to sizes up to 100 nm, which corresponds to the thickness of the films and explains the reported high film roughness. Similar effects were reported for ZnS film formation [55]. In contrast, chelating ligands present during CdS film formation led to reduced surface roughness [166]. Compared to the conventional SILAR technique, increased growth rates and a high degree of orientation of the films were reported.

Recently, a variety of other thin films, including CoS [51], Cu_xS [52], Ag_2S [54], Sb_2S_3 [55, 56], and Bi_2Se_3 [58], have been synthesized by Lokhande et al. by the SILAR technique. Although rinsing steps were included in the process, the reported growth rates of 12–55 nm/cycle exceeded by far the value of a monolayer/cycle, indicating that the film formation could not have been related only to adsorbed ionic layers (see § 2.2.3–2.2.4 for the deposition mechanism). Indeed others have reported reasonable lower values for CuS (0.05–0.3 nm/cycle) or In_2S_3 (0.7 nm/cycle) [53, 57].

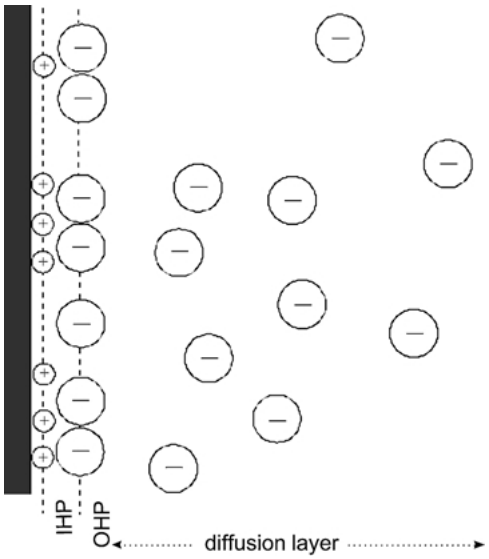

Fig. 3. Stern's model of the electrical double layer in case of specific adsorbed cations. IHP = inner Helmholtz plane, OHP = outer Helmholtz plane.

2.2.3. Deposition mechanism for SILAR sulfide thin films. Consider the deposition of a CdS film by SILAR, using alternating aqueous solutions of $CdSO_4$ and H_2S/NaOH. To exclude homogenous precipitation, specific and strong adsorption of the desired ion on the substrate (and later on the film) is required in each immersion step, followed immediately by rinsing in high-purity deionized water [46, 167]. When the substrate is first immersed in the $CdSO_4$ salt solution, specific adsorption of the cations will occur if the solution's pH is above the substrate's isoelectric point. Thus an electrical double layer is formed at the solid-liquid interface with Cd^{2+} in the inner Helmholtz plane and SO_4^{2-} in the outer, both surrounded by the diffusion layer (Stern's model, Fig. 3). The substrate's surface becomes saturated with respect to Cd^{2+} after a certain time that has to be determined experimentally (or calculated). In the following rinsing step, time must be adjusted so that the residual concentration of Cd in the diffusion layer, $[Cd_r^{2+}]$, is less than $K_{CdS}[H+]/K_{a2}[HS^-]$ (where K_{CdS} is the solubility product of CdS and K_{a2} is the second ionization constant of H_2S) to avoid the precipitation of CdS nanocrystals in the diffusion layer in the subsequent immersion. In that immersion (H_2S/NaOH), sulfide ions (or HS^-) enter the outer Helmholtz plane and sulfate ions diffuse back into the sulfide solution. CdS is formed by reaction between the adsorbed cations (in

the inner Helmholtz plane) and the sulfide ions (in the outer Helmholtz plane) only, and a new electrical double layer is formed by Na^+, HS^-, S^{2-} and OH^- ions. By reasoning similar to that used for the first rinsing step, the following rinsing step has to be suffiently long to minimize the residual [HS^-] concentration.

Klechkovskaya et al. [168] pointed out that, if epitaxy occurs between film and substrate, in wurtzite structures, a layer-by-layer growth mode (or *Frank-van der Merwe* growth) can be assumed. On the other hand, the formation of polycrystalline films implied that the deposition had originated with the formation of many individual, unoriented, three-dimensional growth centers, followed by their coalescence to cover the whole substrate, during which preferred orientation may arise (*Volmer-Weber* growth).

In the mid 1990's, Resch and co-workers [169] started a series of ongoing investigations of the ZnS SILAR process, using atomic force microscopy to determine the growth mechanisms. An AFM liquid cell was used as a flow-through reactor for in-situ measurement of the deposition and results were compared with conventionally grown films. In summary, the growth mechanism seems to be strongly dependent on the substrate used. On (atomically flat) mica, three-dimensional island growth was observed from the beginning of the experiment [170]. On glass, the growth changed after five cycles from two-dimensional to either purely three-dimensional growth or layer-plus-island growth (*Stranski-Krastanow* growth) [170, 171]. On GaAs, ZnS thin films deposited first via three-dimensional growth, but changed to two-dimensional growth, giving flatter films than on mica or glass [172, 173]. On Si(100), the etching of the Si substrate in the basic sulfide precursor solution disturbs the growth process and only very thin and rough films could be formed [174, 175].

The residual stress in SILAR-grown CdS and ZnS films on GaAs was recently analyzed with laser interferometry [173, 176]. Tensile stress (1.4×10^9 (CdS) and 6.9×10^8 N/m^2 (ZnS)) dominated at low thicknesses (30–50 nm) which was related to film-substrate interactions during the initially three-dimensional growth. During further deposition via two-dimensional growth (>60 nm), the surfaces of adjacent crystallites came into contact, resulting in compressive stresses (-2.5×10^9 (CdS) and -5.89×10^8 N/m^2 (ZnS)).

2.2.4. SILAR of oxide thin films. Table 2 lists oxides that have been deposited in thin-film form via SILAR and summarizes the deposition parameters, maximum thicknesses, and growth rates. Whereas sulfide thin films were usually deposited at room temperature, Ristov et al. [29] had to use a heated hydroxide solution (60–80°C) and a cation solution at room temperature (complexed by thiosulfate, which also works as reductant for the Cu^{2+} ions) to deposit micron-thick Cu_2O thin films on glass. Likewise, hot water (95–100°C) was used as the hydrolyzing agent to deposit polycrystalline (hexagonal) ZnO thin films onto glass, quartz and mica substrates [32]. Here, the best film quality was obtained from tetraaminezinc(II) complex solutions, probably reflecting the ability of a complexing agent to control the rate of hydrolysis as in CBD. The films exhibited a strong orientation (*c*-axis perpendicular to the substrate). Doping was achieved by adding a Sn^{2+} salt to the zinc deposition solution.

It should be pointed out that Ristov et al. did not use any rinsing steps after dipping the substrate in the cation and anion solutions respectively. Therefore, their film formation involved (undesired) precipitation in the diffusion layer and not simply adsorbed ions. Additionally, precipitates may have been formed in the solutions due to cross-contamination, as was recently shown by Nair et al. [30], following Ristov's original recipe for Cu_2O thin films. A growth rate of 10 nm/cycle was typical, slowing down after about 20 cycles. Mitra et al. [35] showed that ZnO film growth rates without rinsing steps are 7–25 nm per cycle and that film thicknesses of more than 7 μm can be reached. (For *c*-oriented ZnO, layer-by-layer growth would give a growth rate of $c/2$ per cycle, i.e., 0.3 nm/cycle.) If rinsing steps were included, as done by Jiménez-González and Nair [33], the growth rate was limited to approximately $\sim$2.5 nm per cycle and film thicknesses reached only 20–110 nm but better film quality was obtained.

Heat treatment modifies the crystal structure and the properties of the as-deposited films. Crystalline defects arising from the transformation of $Zn(OH)_2$ films to ZnO during heating to 450°C were believed to cause the increased conductivity (dark- and photo-) of the films [34]. Doping of the ZnO thin films by Ni and Cu was reported [40]. While Ni doping enhanced the *c*-axis orientation of the films during heat treatment and increased the electrical conductivity, Cu doping led to randomization of the crystallites and reduced electrical conductivity.

A significant limitation in SILAR deposition of oxide thin films seems to be that upon repeated treatment of the growing film, which is necessary for the synthesis

Table 2. Oxide thin films deposited via successive ionic-layer absorption and reaction (SILAR).

System				Temperature (°C)						
Oxide	Substrate	Solution A	Solution B	Deposition[b]	As-deposited	Annealing	pH[a]	Growth rate (nm/cycle)	Max. thickness (nm)	Reference
MnO_2	Si	Mn^{2+}	MnO_4^-	20	Amorphous	n.r.	Neutral	~1	~15	[26]
$FeOOH/Fe_2O_3$	Si, SiO_2	Fe^{2+}	H_2O_2/KOH	20	FeOOH	250°C (Fe_2O_3)	8.5	0.5	10	[27]
NiO	Si, quartz	$[Ni(NH_3)_4]^{2+}$	H_2O_2/KOH	20	$NiO_{1-x}\cdot nH_2O$	240°C	8–8.5	0.5	~30	[28]
Cu_2O	Glass	$[Cu(S_2O_3)]^-$	NaOH	60–80	Polycrystalline	Optional	Basic	n.r.	200	[29]
Cu_2O	Glass	$[Cu(S_2O_3)]^-$	NaOH	50–90	Polycrystalline	Optional	Basic	10	450	[30]
CuO	Si	Cu^{2+}	H_2O_2/NH_3	20	$CuO_2\cdot nH_2O$	>220°C	~9	0.3–1.5	22.5	[31]
ZnO, ZnO:Sn	Glass, quartz, mica	ZnO_2^- or $[Zn(CN)_4]^{2-}$	Water	95–100	Polycrystalline	Optional	Neutral	n.r.	850	[32]
ZnO, ZnO:Ni, Cu, Cd	Glass	$[Zn(NH_3)_4]^{2+}$	Water	96	Polycrystalline	Optional	Neutral	2.5	110	[33, 34, 40]
ZnO	Glass	ZnO_2^-	Water	95–100	ZnO (and $Zn(OH)_2$ for films >1 μm)	250°C	Neutral	7–25	>7000	[35–37]
ZnO	Si	Zn^{2+}	H_2O_2/NH_3	20	$ZnO_{2-x}\cdot nH_2O$	200°C	~9.0	0.3–0.9	14	[38]
ZnO	SiO_2, Si, PVC, polycarbonate	$[Zn(en)_3]^{2+}$	H_2O_2/NH_3	20	$ZnO_2\cdot nH_2O$/ $Zn(OH)_2$	200–800°C	8.8	0.15–0.25	~60	[39]
Tl_2O_3	Si, quartz	Tl^+	H_2O_2/KOH	20	$Tl(OH)_3/Tl_2O_3$	n.r.	Basic	0.5	4.5	[41]
SnO_2	Si	Sn^{2+}	H_2O_2/KOH	20	$SnO_2\cdot nH_2O$	n.r.	8–9	0.8	7.2	[42]
$LaNbO_x$	Si	La^{3+}	$[NbO_3(O_2)]^{3-}$	18–20[c]	Amorphous	400°C	4.0	0.75	11	[43]
Ln_2O_{3-x} (Ln = Y, La, Eu)	Si	Ln^{3+}	H_2O_2/NaOH	20	$Ln(OH)_2(OOH)$	400°C	9	1.2	12	[45]
CeO_{2+x}	Si, SiO_2, quartz	Ce^{3+}	H_2O_2/NH_3	20[c]	Amorphous	100–500°C	~9	0.3–1.5	300	[44, 178]

[a]pH of solution B.
[b]Hydrolyzing temperature (solution B). Solution A is kept at room temperature.
[c]Deposition starts with boiling solution A in first deposition cycle.

of the next layer, the film is redissolved in the solution of the metal salt. Therefore, Tolstoi suggested the use of a metal salt in a lower oxidation state and to oxidize the metal ions during film formation. MnO_2 was formed from Mn^{2+} and MnO_4^- solutions [26], while FeOOH, Tl_2O_3 and SnO_2 were formed by oxidation with hydrogen peroxide of Fe^{2+}, Tl^+ or Sn^{2+} respectively [27, 41, 42]. In other cases, when only one stable metal ion oxidation state exists, metal peroxide layers were formed by hydrogen peroxide treatment, including ZnO_{2-x} [38, 39], CeO_{2+x} [44], NiO_{1-x} [28], copper peroxide [31], and Y, La and Eu hydroperoxide [45]. CuO_2/BaO_2 [177] and $CeO_{2+x}/LaO_{1.5+x}$ [178] mixed nanolayers were grown by sequential exchange of the cation solutions. A third approach was used to synthesize binary peroxides (e.g., $LaNbO_x$): Here, nanolayers were formed by interaction of a soluble metal peroxicomplex with the second metal ion [43]. In contrast to the work mentioned above, film formation was always done at room temperature and rinsing steps were included. In most cases, the as-deposited peroxide or hydrated oxide films could be transformed to the corresponding oxide films by heat treatment.

2.2.5. Applications. In contrast to CBD, none of the SILAR-grown thin films has reached commercial application yet. Recently, the use of ZnO thin films as gas sensors was demonstrated [36, 37]. Further potential applications include use of SILAR-grown films in optoelectronic or electroluminescent displays [32, 162], in light-emitting devices [48, 49], in heterojunction solar cells [34, 158] or in field-effect transistors [158].

2.3. Liquid-Phase Deposition (LPD)

2.3.1. Introductory remarks. The term "liquid phase deposition" refers to the formation of oxide thin films from an aqueous solution of a metal-fluoro complex $[MF_n]^{m-n}$ which is slowly hydrolyzed by adding water, boric acid (H_3BO_3) or aluminum metal. While the addition of water directly forces precipitation of the oxide, boric acid and aluminum act as fluoride scavengers, which destabilizes the fluoro complex and forces the oxide precipitation. In the case of water and boric acid, the addition is done either all at once [179–182], or dropwise [183–188]. The aluminum, as a solid reacting much more slowly than a solvated species, will lead to similar results as the dropwise addition. Compared to the formation of oxide films by CBD, this step allows much better control of the hydrolysis reaction and of the solution's supersaturation. Additionally, film formation is done from strongly acidic solutions in contrast to the usually basic or slightly acidic CBD baths. These justify the use of a new term despite obvious similarities to the CBD technique.

Unlike CBD and SILAR, LPD was developed originally (and is still used exclusively) as a route to oxide films. It was first reported as a new process for silica coatings [179], for which LPD is still most widely used. The next section (§ 2.3.2) describes the general mechanisms of the LPD technique, followed by a review of the deposition of silica (§ 2.3.3) and other oxides (§ 2.3.4). Finally, § 2.3.5 discusses applications of LPD-grown films.

2.3.2. General description. Simplified, the LPD technique is based on the overall equilibrium reaction

$$H_{(n-m)}MF_n + m/2\,H_2O \Leftrightarrow MO_{m/2} + nHF \quad (14)$$

where m is the charge of the metal cation. According to this reaction, the equilibrium will be shifted towards the oxide if the concentration of water is increased or if the hydrogen fluoride concentration is decreased via addition of fluorine scavengers such as boric acid [179] or aluminum metal [189]:

$$H_3BO_3 + 4HF \Leftrightarrow BF_4^- + H_3O^+ + 2H_2O \quad (15)$$

$$Al + 6HF \Leftrightarrow H_3AlF_6 + 1.5H_2 \quad (16)$$

Of these three techniques, the addition of boric acid (usually 0.1 M) is the most common. Boric acid functions not only as a fluorine scavenger, but it also shifts reaction (14) to the right by producing water. In this simplified description, homogeneous nucleation and colloid formation occur if the oxide's solubility limit is reached, and thin films are formed via attraction and attachment of colloidal particles.

Certain characteristics of films deposited by LPD cannot be explained by reactions (14)–(16). For example, the films contain a uniformly distributed fluorine content (typically ~5 atom%), which is usually attributed to the incorporation of intermediate complexes containing metal and fluorine into the growing film. Secondly, the films form preferentially on SiO_2-covered substrates [179, 184, 185], which suggests that hydroxyl groups (which typically terminate a silicate surface in water-containing environments) are necessary on the substrate for deposition to occur. Models for

the deposition of silica films will be explained in more detail below. Aspects of these models hold for films of other oxides also. However, none of these models has yet been confirmed by experiment.

In the archetypical LPD process, hydrofluorosilicic acid (H_2SiF_6) is hydrolyzed to form silica (SiO_2). Lee and co-workers [181, 182, 190] proposed that intermediate, partially hydrolyzed species ($SiF_n(OH)_{4-n}$ with $n < 4$) form by the reaction:

$$H_2SiF_6 + (4-n)\ H_2O \Leftrightarrow SiF_n(OH)_{4-n} + (6-n)\ HF \tag{17}$$

These intermediate species would react with the surface (either -OH or -F groups, depending on the overall HF concentration) and form the film. Homma et al. [184, 185] also proposed that the hydrofluorosilicic acid is partially hydrolyzed, but that fluorine-containing siloxane oligomers are formed. These oligomers could be adsorbed onto the substrate surface where catalytic dehydration (and bonding) between the oligomers and the surface-bound hydroxyl groups occurs (catalyzed by the fluorine).

Yeh et al. [183] proposed that silica is dissolved beyond its solubility limit in the form of $[SiF_6 \cdot SiF_4]^{2-}$. Adding water, a nucleophile, attacks the bridging fluorines in this complex, leading to the formation of $SiF_4(OH)_2^{2-}$ and eventually (after protonation in the acidic solution) SiF_4. Finally hydrolysis should form a silicic monomer $Si(OH)_4$ that spontaneously starts to polymerize. Since the concentration of this polysilicic acid remains low, network formation inside the solution is prevented and the polymer is instead adsorbed on the surface, followed by the Si—O—Si bond formation. The as-deposited oxide might be still attacked by HF, explaining the fluorine content in the films.

2.3.3. LPD of silica thin films. LPD-SiO_2 was deposited on SiO_2 substrates (glass, CVD grown films, native oxide on silicon), but no deposition occurred on photoresists, teflon or tungsten [184], and Si_3N_4 [191]. Substrate treatment prior to deposition to increase the amount of surface OH groups seems to be an important step in the LPD process. Lee et al. [182, 190] pointed out that deposition on an HF-pretreated silicon wafer is only possible below a critical HF concentration in the deposition solution. This allows reaction between surface Si-H and water to form surface Si-OH (and probably Si-F by subsequent reaction with HF). Likewise, film deposition was only successful on the semiconductors GaAs and HgCdTe if the substrate surfaces were wet-chemically treated prior to deposition to enrich them with surface OH groups [192–194].

Transmission electron micrographs indicated that the films are completely amorphous [180]. Atomic force microscopic studies revealed a surface roughness below 0.5 nm [195]. The growth rate is typically linear with time (0–6 h) or temperature (30–50°C) and in the range of 10–340 nm/h (Table 3). However, evaporation at higher temperature leads to significant concentration changes in the solution and undesired formation of SiO_2 precipitate.

To set up the deposition solution, usually a suspension of industrial grade hydrofluorosilicic acid and a silica source (silica, silica gel, silicic acid) is stirred at 23–35°C for several hours, whereby free hydrofluoric acid reacts with the silica source and a saturated solution is formed. Chang et al. [59] differentiated between two experimental routes: adding water after filtering of the silica source to reach a supersaturated H_2SiF_6 solution (1.5–3.8 M) (route I) [180–183, 191, 195–198]; or diluting the hydrofluorosilicic acid before adding the silica source (route II) [179, 184–188, 199]. In the latter route, the added silica could nucleate the precipitation, depleting the growth solution of SiO_2. Note that after filtering off the silica source, deposition occurred even without adding boric acid or water [181, 182]. That the deposition rate is indeed higher for solutions prepared by route I was experimentally shown by Chou and Lee [182].

Yeh and co-workers [196, 200] were able to control the fluorine content of the as-deposited films by adding different amounts of water to the (boric acid-free) deposition solution. By increasing the amount of water, the fluorine content linearly decreased from 6.25 to 1.86 atom-%, due to the resulting reduced (thus, less aggressive) HF concentration. They reported that thermal annealing of the as-deposited films for one hour under nitrogen at $T \geq 700$°C resulted in densification and total fluorine loss, and that LPD oxide annealed at 1000°C became similar to thermal SiO_2. In contrast, Homma and Murao [185] detected an average concentration of 3.5 atom-% fluorine after annealing at 900°C for the same duration. Chou and Lee [201] pointed out that the fluorine impurity in the as-deposited silica films leads to degradation of the properties during heat treatment at 400–600°C, because undesired dangling bonds remain in the silica network upon removal of the fluorine. However, thermal annealing of an LPD silica film previously covered by an aluminum film (i.e.,

Table 3. Silica thin films deposited via liquid phase deposition (LPD).

Substrate	SiO_2 source	Route[a]	Additive	Dep. temp. (°C)	pH	Growth rate (nm h^{-1})	Max. thickness (nm)	Reference
Glass	Silica gel	II	H_3BO_3	30–40	Acidic	8–24	93	[179]
Si	Silica gel	II	H_3BO_3	35	Acidic	25–50	235	[199]
CVD-SiO_2	Silica	II	H_3BO_3[b]	35	Acidic	20	800	[184, 185]
SiO_2/Si	Silica	II	H_3BO_3[b]	20–60	Acidic	10–170	∼500	[186–188]
Si, SiO_2/Si	Silica	I	H_2O[b]	15–40	Acidic	5–110	170	[183, 196, 197]
Si, SiO_2/Si	Silicic acid	I+II	(H_3BO_3)	30–50	Acidic	50–250	200	[181, 182]
GaAs	Silicic acid	I	H_3BO_3	30–40	Acidic	0–130	n.r.	[193, 194]
HgCdTe	Silicic acid	II	H_3BO_3[b]	30–45	Acidic	170	n.r.	[192]
SiO_2/Si	Silicic acid	I	H_3BO_3	50	Acidic	55–340	n.r.	[59]
SiO_2/Si	Silicic acid	I	H_3BO_3	27–40	Acidic	67–140	155	[180]
SiO_2/Si	Silica gel	I	H_3BO_3	40	Acidic	∼60	∼180	[191, 198]
InP	Silicic acid	II	$H_3BO_3^b$ or H_2O[b]	40	Acidic	45–105	107	[303]
SiO_2/Si, glass	Silica gel	II	Al	30–35	Acidic	80	240	[189]
Spin-on-glass	(H_2SiF_6)	–	Al	23	Acidic	42–50	1157	[213]
SiO_2/Si	Silica gel	TD-LPD	–	35–60	Acidic	n.r.	1000	[206]
Si, SiO_2/Si	Silica	TD-LPD	–	35	Acidic	15–130	240	[195]
SiO_2/Si	Silica	TD-LPD	–	15–40	Acidic	2–120	400	[207]
SiO_2/Si	Silica gel	I	H_3BO_3, NH_4OH[c]	40	Acidic	52–160	200	[304]

[a] See text for description.
[b] Added stepwise.
[c] SiON thin film formation.

the conductor) improved the materials' properties. The authors suggested that the aluminum reacts with residual water in the silica thin film, forming alumina (that will become part of the gate insulator) and hydrogen:

$$2Al + 3H_2O \Leftrightarrow Al_2O_3 + 3H_2 \qquad (18)$$

The hydrogen could then diffuse to the SiO_2/Si interface and passivate any dangling bonds generated during the annealing.

Likewise, thermal oxidation in dry oxygen at 900°C was applied to LPD silica films to passivate the defects and vacancies introduced during annealing [202, 203]. Plasma treatment [204] including H_2 or O_2 and CO_2 laser annealing [205] have also been shown to be effective.

A more recent approach in SiO_2-LPD is to control the degree of supersaturation of the deposition solution by altering the difference between the solution preparation temperature and the deposition temperature, instead of adding supersaturation initiators or fluoride scavangers (temperature-difference based LPD). Kawahara et al. [206] prepared the solution at −3°C and warmed it up to 35–60°C. This formed silica films 0.1–1 μm thick in a single dip and over 10 μm thick by repeated depositions with fresh solutions. Chanthamaly et al. [195] and Yeh et al. [207] prepared their deposition solution at 2–3°C or 0°C respectively, leading likewise to high growth rates at the deposition temperature (15–40°C). The authors suggested that the HF molecules are ionized at low temperature, leading to a less reactive solution that becomes supersaturated upon warming. The fluorine concentration in such films, typically ∼7–9 atom-%, is higher than in films prepared by conventional LPD.

2.3.4. LPD of other oxide thin films. The LPD technique is in principle suitable for the deposition of other oxides of metals that form stable fluoride complexes. This was first shown in 1996 independently for titania and zirconia thin films by Deki et al. [60] and Yao et al. [67], respectively. Table 4 lists the oxides that have been deposited by LPD and summarizes the

Table 4. Non-silica oxide thin films deposited via liquid phase deposition (LPD).

System			Temperature (°C)						
Oxide	Substrate	Additive	Deposition	As-deposited	Annealing	pH	Growth rate (nm h^{-1})	Max. thickness (nm)	Reference
TiO_2	Glass	H_3BO_3	30	Anatase/amorphous	600	Acidic	12–20	~900	[60, 61, 63]
TiO_2	Glass, ITO/glass	H_3BO_3	25	Amorphous	300–500	Acidic	~3	160	[65]
TiO_2/SiO_2	SiO_2/Si	H_3BO_3	40	Amorphous	n.r.	Acidic	36	100	[66]
TiO_2	Glass, polymers	(H_2O)	40–70	Anatase	300	1.0–3.1	70–340	170	[64]
ZrO_2	Glass	H_3BO_3	30	Polycrystalline	None	Acidic	n.r.	n.r.	[67]
V_2O_5	Glass	Al	30	Amorphous	400	Acidic	n.r.	n.r.	[68, 69]
β-FeOOH, α-Fe_2O_3	Glass	H_3BO_3	30	β-FeOOH	600 (α-Fe_2O_3)	Acidic	~25	~500	[70]
$NiFe_2O_4$	Glass	H_3BO_3	30	Amorphous	600	Acidic	n.r.	n.r.	[62]
$LnMO_3$(Ln = La, Nd; M = Cr, Mn, Fe, Co)	PET	H_3BO_3	30	Perovskite	None	Acidic	n.r.	n.r.	[71, 72]
SnO_2	Glass, SiO_2/Si	(H_2O)	40–80	Amorphous	300	Acidic	2–20	~500	[73]

deposition parameters, the growth rates and maximum achieved film thicknesses.

Deki and co-workers [60] deposited titania thin films from an aqueous ammonium hexafluorotitanate solution by the addition of boric acid. As-deposited films consisted of nanocrystalline anatase embedded in an amorphous, flourine- and nitrogen-containing phase. Growth rates were monitored with a quartz crystal microbalance to be between 12 and 20 nm/h, which is lower than what is usually reported for LPD silica films (Table 2) [61]. Annealing at 600°C in air led to fully nanocrystalline anatase thin films with an average crystallite size of ca. 120 nm. (If the deposition solution was made by saturating a hexafluorotitanic acid solution with titania oxide powder at room temperature (i.e., similar to LPD-SiO_2), the released hydrofluoric acid reacted with the silicon substrate, leading to films containing SiO_2 and TiO_2 [66].)

The same group [68, 69] formed vanadium-containing films by dissolving vanadia in hydrofluoric acid and using aluminum metal as fluorine scavenger. However, the aluminum also reduced the vanadium ions from pentavalent to tetravalent. The as-deposited films consisted of amorphous vanadium (IV) oxide. Subsequent annealing in air at 400°C led to crystallization and oxidation to V_2O_5, whereas annealing under inert atmosphere at 400°C transformed the films to monoclinic VO_2 with partial [001] orientation.

Iron oxyhydroxide (β-FeO(OH)) thin films were deposited from a solution of iron oxyhydroxide in $NH_4F{\cdot}HF$ [70]. The films were polycrystalline, and their orientations were either random or with [211] perpendicular to the substrate, depending on the boric acid concentration used. After air annealing at 600°C, α-Fe_2O_3 with partial [110] orientation was detected. If nickel nitrate was added to the growth solution, nickel was incorporated in the film [62], and the annealed films showed diffraction peaks (though weak) of nickel ferrite.

Yao et al. [67, 72] formed ZrO_2 thin films from sodium hexafluorozirconate (or a solution of zirconia in hydrofluoric acid) by adding boric acid. Likewise, the same authors deposited $LnMO_3$ (Ln = La, Nd; M = Cr, Mn, Fe, Co) from a solution of the corresponding perovskite in hydrofluoric acid [71, 72]. In all cases, XRD patterns of the as-deposited films indicated the formation of crystalline phases and SEM micrographs showed connected aggregates with an individual size up to several microns. No more details on the film morphology were reported.

Experiments have been expanded to solutions in which the metal ions are only partially complexed by fluorine (in which cases the similarities to CBD are more obvious). Tsukuma et al. [73] formed tin(IV) oxide thin films from a solution of SnF_2 in water. After subsequent annealing in air at 300°C, pure SnO_2 (rutile structure) was observed. Titania thin films have been deposited using a supersaturated aqueous solution of titanium tetrafluoride [64]. Film formation was related to suppressed hydrolysis by the stability of Ti—F bonds, leading to heterogeneous nucleation on the substrate. In contrast to Deki's earlier results [60], the as-deposited films were essentially nanocrystalline (~20 nm anatase) with a preferred (001) orientation. The authors suggested that an optimal fluorine content (here ~7 mol-%) promotes the crystallinity of the films (via moderate polymerization) while more or less fluorine inhibits the formation of an ordered structure.

2.3.5. Applications. While applications of non-silicate oxides deposited via LPD have only been suggested, LPD-grown silica has been widely tested for application in integrated circuit processing and metal-oxide-semiconductor (MOS) technology. Conventional gas-phase deposition techniques have several shortcomings that explain the interest in a new deposition technique: Large area applications are limited by the necessity of vacuum equipment. The low temperatures of the LPD process reduce the problems of diffusion and dopant redistribution that occur in higher-temperature processes, allowing the use of substrates that are less thermally stable (e.g., soda lime silicate glass). Incorporation of small amounts of fluorine, which occurs intrinsically in LPD, has been suggested to improve the electric characteristics of ultrathin silica films. Because of the fluorine incorporation, the tensile stress of as-deposited films was found to be low (20–83 MPa) [185, 197], another advantage for integrated circuit technology.

Additional advantages arise from the selectivity of the process. Because LPD silica selectively deposits on SiO_2, but not on photoresists, Horiuchi et al. [208] were able to simplify the number of masking sequences in the complementary metal-oxide-semiconductor (CMOS) process from 13 to 7. Yeh and co-workers [209] pointed out recently the promising results of manufacturing contact holes by selective LPD instead of applying reactive ion etching, which usually causes plasma damage defects. Homma et al. [184, 185] showed that the selectivity is useful to planarize trenches between

tungsten wires previously grown via CVD. This enabled them to achieve fully planarized multilevel interconnections, an essential step in the fabrication of high density ultralarge scale integrated devices. To reduce the cost of liquid crystal displays (LCDs) with high resolution and high pixel density, Yeh et al. [187, 188, 210, 211] and Chou et al. [201, 212] successfully applied LPD silica to the fabrication of polysilicon thin film transistors.

Fluorinated silicon oxide is also a highly attractive layer material for manufacturing optical waveguide structures, due to its lower refractive index compared to silica. The optical properties of LPD-"SiOF" and spin-on-glass layers in such structures have recently been tested [213]. The experimentally found low transmission loss, the low deviation of the refractive index with film thickness (<0.35%), and the low water content (1.8 wt-%) would be suitable for the application of LPD-"SiOF" films in optical waveguide structures.

Further application for LPD silica thin films is found in MOS solar cells. Here, very thin layers (<2 nm) are desired to enable sufficient tunneling current through the insulator. While this is in general difficult to achieve, Lee and Hwu [214, 215] described a solar cell with 18.9% efficiency that contained a silica film ~5 nm thick grown via LPD on unoxidized silicon. Without the native oxide present, the initially deposited silica seems to seed further growth, leading to boundary formation between silica domains. These provide a path for trap-assisted tunneling currents that are sufficiently high for solar cell applications.

2.4. *Electroless Deposition (ED)*

2.4.1. General description. The technique of electroless deposition (ED) of ceramic thin films evolved from electroless plating of metal thin films. The latter technique was first reported in 1946 and has been in continuous use and development since then [216]. Both processes (like all those reviewed here, and in contrast to the older technique of electroplating of metal films) produce films without use of a counterelectrode nor connections to an external electrical power source. Several processes that fit this description and that produce non-metallic films have been called "electroless deposition" in the literature. However, three additional characteristics distinguish electroless plating:

1) a change in the oxidation state of the metal cation (dissolved in aqueous solution) to an insoluble state (which in electroless plating is the neutral metallic state);
2) the participation of the deposition surface (the substrate and, later, the film) in the redox process, usually as a path for transfer of electrons from the site of an oxidation to the site of a reduction;
3) the need for catalysis to initiate and sustain the process.

To maintain consistency in terminology, the term "electroless deposition" will be applied here only to depositions which demonstrably or apparently exhibit these three characteristics.

A discussion of the role of catalysis in electroless plating of metals may serve to clarify the distinctions between ED and the other techniques discussed in this paper. In its original form, electroless plating produced metal films on substrates that were themselves not only metallic but catalytic to the deposition process (e.g., steel, palladium, nickel, cobalt, or rhodium). Metals such as copper or brass that are not catalytic but are also not poisonous to catalysis can be "activated" for subsequent electroless plating by immersion in an aqueous solution of $PdCl_2$ and HCl. If the coating itself exhibits adequate electrical conductivity, the substrate can be an electrical insulator; such substrates can be made catalytic by nucleation in a colloidal palladium suspension, or by a 2-step process of sequential immersion in an aqueous $SnCl_2$/HCl "sensitizer" and a $PdCl_2$/HCl activator. Once the deposition is initiated, the metal film itself must catalyze any further growth ("autocatalytic electroless deposition").

In most other respects ED resembles CBD, particularly in the use of specific oxidizing or hydrolyzing agents to drive the formation of the desired solid phase. Particle sizes of 20–200 nm appear to be typical for this technique, and the films are mostly unoriented. Other results from the literature on ED of oxide films are summarized in Table 5.

2.4.2. ED of oxide thin films. Mindt [74, 79] pointed out in 1971 that electrochemical reactions to form solid oxide films from liquid electrolytic solutions could be caused to occur without the application of electrical current if a suitable oxidizing agent was present in the solution. The reactions that he studied in particular involved an increase in the oxidation state of the metal at room temperature: $Pb(II)_{aq}$ to Pb(IV) oxide; $Tl(I)_{aq}$ to Tl(III) oxide; and $Mn(II)_{aq}$ to Mn(IV) oxide. The corresponding reduction was of aqueous peroxydisulfate (persulfate), $S_2O_8^{2-}$, to sulfate, SO_4^{2-}.

Table 5. Oxide thin films deposited via electroless deposition (ED).

System		Temperature (°C)						
Oxide	Substrate	Deposition	As-deposited	Annealing	pH	Growth rate (nm h^{-1})	Max. thickness (nm)	Reference
MnO_2	Glass	25	Amorphous	None	5–8	n.r.	500	[74]
$La_{1-x}MnO_3$	YSZ[a]	25	Amorphous	800	4–6	40	1,000	[75]
ZnO	Glass	50	Polycrystalline	None	6.2	100–610	2,000	[76, 77]
In_2O_3	Glass	60	$In(OH)_3$	200–300	3	130–700	1,000	[78]
Tl_2O_3	Glass	25	Polycrystalline	None	8	n.r.	10,000	[74]
α-PbO_2	Glass, SiO_2 glass, ceramics, Ta_2O_5	25	Polycrystalline	None	5–10	10–4,560	1,000	[79]

[a]YSZ: yttria stabilized zirconia.

Ammonium acetate was used as the supporting electrolyte. As a catalyst for these reactions, $AgNO_3$ was added to the bath. (Raviendra and Sharma [21] credited the addition of Ag^+ with improving the adherency of the films.) Mindt emphasized the importance of the deposited film being electrically conductive; otherwise, both the anodic and cathodic reactions must occur at the same place to enable the necessary transfer of electrons. His films exhibited values of electrical conductivity of 33–500 Ω^{-1} cm^{-1} for PbO_2 (deposited at pH 10 and 7, respectively), 2000 Ω^{-1} cm^{-1} for Tl_2O_3, and 5×10^{-5} -2.5×10^{-3} Ω^{-1} cm^{-1} for MnO_2 (deposited at pH 6.3 and 8, respectively). These values were high enough that insulating substrates (glass slides) could be coated. (The intended application was electrodes for metal oxide capacitors.) The resulting films of PbO_2 and Tl_2O_3 consisted of the stable crystalline forms, whereas the MnO_2 films exhibited no x-ray diffraction peaks.

Mindt's work with Mn oxides provided a starting point over twenty-five years later for Sasaki et al. [75], who used ED to deposit a precursor to $LaMnO_3$ on yttria-stabilized zirconia disks at room temperature. This manganite is used as the air electrode in high-temperature solid oxide fuel cells. They used the 2-step sensitizer-plus-activator pretreatment of the substrate described above. To the source solution they added sodium acetate as a supporting electrolyte, and silver nitrate as a catalyst for the oxidation by ammonium persulfate of Mn(II) in solution to Mn(IV) in the film. Though the starting La/Mn ratio in the solutions ranged from 10 to 1000, the ratio in the deposited film was far less than 1 unless sodium acetate and silver nitrate were used. The amorphous deposit converted to a 1-μm-thick film of the desired crystalline manganite, with grain size of 0.2–0.5 μm, on heat treatment in air at 800°C. This is 400°C lower than the usual ceramic preparation technique.

Izaki's work on ZnO [76, 77] and In_2O_3 films [78] bears several superficial resemblances to ED as it is defined here. He used the two-step pretreatment of the substrate described above. Gas evolution was observed at his substrates during deposition, as in electroless metal plating, where hydrogen gas is always evolved. The nitrate counteranion from his metal salts effectively served as the oxidizing agent, when triggered by addition of an organic aminoborane (di- or trimethyl aminoborane), which are common reducing agents in electroless metal plating. Still, no change in the oxidation state of the cations was observed during deposition, and it is doubtful that the films exhibited significant electrical conductivity at the temperature of deposition (50–60°C). Therefore, the deposition was probably actually more like CBD. ZnO was crystalline (wurtzite structure) as deposited, while cubic In_2O_3 films were obtained after heat treatment of as-deposited crystalline $In(OH)_3$ films. The envisioned applications included liquid crystal displays and photovoltaic devices.

Some of the CBD studies by Varkey and Fort (Table 1) involve an oxidation of the metal (Ag(I) to Ag(II) oxide [11]; Co(II) to cobalt (III) oxyhydroxide [7]). These oxidations, however, took place in the bulk solution rather than at the substrate. Further, no catalyst was used. Therefore, this work is regarded here as CBD.

3. Variations on the Main Techniques

3.1. Photochemical Deposition (PCD)

If sulfide thin films are formed by chemical bath deposition, the process, once started, is difficult to control

because the sulfur-providing reaction proceeds autocatalytically. In contrast, a photochemical reaction to provide the sulfide would be more controllable and would allow selective deposition via application and control of an external light source. Using this idea, Goto et al. [217–220] recently developed a photochemical deposition (PSD) technique. Micron-thick CdS and ZnS thin films were formed from acidic salt solutions on glass, quartz and silicon wafers at 20–35°C in the presence of thiosulfate. The as-deposited CdS thin films were found to be mainly polycrystalline and cubic. The ZnS thin films, in contrast, were amorphous and contained elemental Zn due to reduction of the metal ions by thiosulfate.

In contrast to conventional CBD, these depositions were carried out under acidic conditions: When the pH is too low for spontaneous formation of CdS and too high for precipitation of colloidal sulfur (pH = 3–8), illumination ($\lambda = 254$ nm) can be used to initiate and sustain (i.e., control) the formation of CdS. Photoactivated redox reactions for sulfide formation were suggested to be dominant.

To avoid nucleation in the solution, as pointed out by Goto et al., the substrate had to be placed sufficiently near to the light source. If the distance exceeded ~10 mm, the UV light was absorbed by the solution, and the spontaneously formed CdS diffused away without film formation. This also explains why only illuminated regions of the substrate were coated, which offers the possibility of optically patterning (or, by rastering a laser, "writing") the film, with or without the use of photoresist.

In photo-assisted CBD of CdSe films from conventional basic solution, Nemec et al. [221] controlled the nanocrystal radii between 1.9 and 10 nm by selecting a proper light intensity and/or wavelength during deposition. The authors suggested that the illumination caused electron-hole pair formation on each crystallite, which modified the chemical equilibria compared to conventional CBD.

Photochemistry has also been applied to modify the LPD process [222]. A standard LPD solution was prepared from hydrofluorosilicic acid, silicic acid and boric acid. At constant boric acid concentration, the deposition rate increased linearly with increasing light intensity. This effect was more obvious at high boric acid concentration. However, the reported maximum deposition rate (75 nm/h) is in the limit of the standard LPD technique (see Table 3) and no patterning capability is connected with this photochemical process. The mechanisms behind this process remain unclear. The authors attributed the higher deposition rate to UV-absorption by SiF_6^{2-}, leading to higher concentrations of intermediate species (see Eq. (13)), for example.

3.2. Applying External Forces or Fields

As discussed in § 2.1, the formation of precipitates in the deposition solution is a significant drawback in chemical bath deposition if it leads to porous, loosely attached films. Recently, Choi et al. [223] reported that ultrasonic agitation suppressed the agglomeration of formed colloidal particles. Therefore, compact and smooth thin films were formed without suppressing the homogeneous nucleation, i.e., from solutions that would otherwise be considered non-optimal. Films thicker than 150 nm were not obtained, regardless of the Cd concentration, but the deposition rate increased without losing film quality. The average size of the CdS grains decreased from 12–15 nm to 2–5 nm, which was attributed either to the local high pressure caused by ultrasonication or to a promotion of the nucleation. It might not, however, be necessary to invoke such additional effects: even without ultrasonic agitation, films formed from colloidal particles usually consist of smaller grains than films formed by heterogeneous nucleation (§ 2.1.4). Therefore, simple colloidal growth might be operative here as well.

Vásquez-Luna et al. [224–227] recently investigated the influence of applying magnetic or electric fields on the CBD of CdS thin films. In a magnetic field of 0.04 Tesla perpendicular to the substrate, a smaller average grain size of the crystallites (30 nm instead of 73 nm) was observed. This effect was less pronounced if the magnetic field was parallel to the substrate. While smaller grain sizes are usually obtained at lower kinetic energy of the ions (due to the increased probability of being captured by a nucleation center), the authors suggested that the magnetic field decreased the kinetic energy by increasing the amount of collisions. Electrical fields also influenced the crystallinity and orientation of the film: When the field was applied perpendicular to the substrate, CdS grains grew preferentially along the [111] direction, and with this axis parallel to the applied field.

3.3. Ferrite Plating

For the synthesis of films of magnetic iron oxides (mostly spinel ferrites, MFe_2O_4, where M represents

one or more of any of several cations), Abe and co-workers developed a technique that they called "ferrite plating". One embodiment of this technique entails the application of current from an external source, which falls outside the scope of this paper. The other variations of the technique resemble electroless deposition as defined above, because an essential step in the process is inducing an increase in the oxidation state of the principal cation in the starting solution, in this case Fe from II to III. However, unlike ED, this oxidation occurs in solution by means of an added oxidizing agent, rather than at the substrate. Also unlike ED, ferrite plating does not require catalysis. The inventors postulated that film formation requires adsorption of solvated iron species onto hydroxyl or carboxylate groups on the substrate (or hydroxyl groups on the growing film). In these respects, ferrite plating resembles CBD. (The reported role of surface hydroxyl groups in ferrite plating is reminiscent of the role of cadmium hydroxide in CBD of CdS films.) Of the extensive literature on ferrite plating by Abe and co-workers (see also reviews ref. [228, 229]) and a handful of other research groups, those papers which report film deposition without the use of 1) externally applied current, 2) spraying or dripping of the solution, or 3) hydrothermal conditions are summarized in Table 6.

Ferrite plating was described in its original form in the early 1980's [230–232]. Solutions of Fe (II) chloride (alone or with Co (II) chloride) at 70°C were oxidized by adding nitrate ions or by bubbling air through the solution. The pH was held constant at a value around 7, depending on the intended composition of the deposit, with metered additions of NaOH. To try to confine oxidation of the solution to the vicinity of the substrate, and thereby to avoid bulk precipitation in the solution (which would occur at pH values above ~7.5–8), the air was bubbled into the solution near the substrate. Magnetite films could be formed directly on stainless steel. Films could be deposited on copper if it was pre-oxidized (to provide the necessary hydroxyl-terminated oxide surface), and on polyethylene terephthalate (PET) if it was first plasma-treated (or coated with Cu which was then oxidized).

The deposition rate for simple spinels in the ferrite plating process was 3–10 nm min^{-1}. Higher deposition rates could be achieved if the solution was driven to bulk precipitation, but this degraded the surface quality of the films. (Abe and co-workers have repeatedly asserted that FP achieves the best films when only heterogeneous nucleation occurs.) To increase the growth rate, they developed a liquid flow deposition (LFD) technique (§ 3.5) starting in the late 1980's [233, 234]. (In fact, the LFD papers described below (§ 3.5) cite the FP literature as the source of the design of the LFD apparatus.) Two aqueous solutions, in this case $FeCl_2$ (to obtain magnetite; $FeCl_2/CoCl_2$ to obtain cobalt ferrite) and $NaNO_2$, were filtered, combined, adjusted (using ammonium acetate, CH_3COONH_4) to a pH of 7.0, and flowed in a layer 0.5 mm thick at a rate of 11 ml min^{-1} past a glass substrate maintained at a temperature of 90°C. This approach achieved an increase in the deposition rate to 30 nm min^{-1}, while also achieving improved film quality. The authors attributed these improvements to the constancy of the composition of the solution achieved in this design, and to the rinsing away of ferrite particles formed in the bulk of the solution. The films were crystalline as deposited, with a columnar growth habit and a grain size of about 0.1 μm. The magnetite films exhibited (100) orientation, whereas the cobalt ferrite films had (111) orientation. These authors reported deposition also onto GaAs substrates that had first been coated with a CVD SiO_2 layer [235]. Lee et al. [236] later achieved growth rates of cation-deficient magnetite films of 20 nm min^{-1} using LFD and the water-soluble polymer dextran $[(C_6H_{10}O_5)_{1200-1800}]$ as a catalyst and oxidant for the formation of the spinel.

This improvement in deposition rate was not sufficient for the intended application (a microwave circulator requiring a ferrite film 10 μm thick). By irradiating the glass substrate with light from a Xe lamp at a density of 450 W cm^{-2}, a further 10-fold increase in deposition rate was obtained (to 320 nm min^{-1}) [237]. The authors noted that the illumination increased the local temperature at the substrate above 100°C, as evidenced by the release of bubbles. Previous work had shown that simply heating the solution uniformly to such temperatures could not increase the growth rate. They concluded, therefore, that the induced temperature gradient at the substrate-solution interface enhanced the local rate of electron transfer and led to local convection currents, effects which together accounted for the enhanced growth rate under optical irradiation [238–240]. Still higher growth rates (660 nm min^{-1}) were achieved using an Ar laser as the light source to deposit magnetite films, which also allowed maskless photopatterning.

Control of the composition of the film in mixed-cation solutions was difficult because of differences in the solubility-pH characteristics between the cations,

Table 6. Oxide thin films deposited via ferrite plating[a].

System		Temperature (°C)						
Oxide	Substrate	Deposition	As-deposited	Annealing	pH	Growth rate (nm h^{-1})	Max. thickness (nm)	Reference
Fe_3O_4, $CoFe_2O_4$	Cu, PET[b], Fe_3O_4 on steel	70	Spinel	None	6–11	180–600	800	[230–232]
Fe_3O_4 $Co_xFe_{3-x}O_4$	Glass, sapphire, spinel, PET, PTFE[b]	55–90[c]	Spinel	None	6.9–7.3	960–2,400	800	[233, 234, 305, 306]
Fe_3O_4	Glass	~100[d]	Spinel	None	6.6	9,000–19,200	~20,000	[237, 238]
$Fe_{3-x}M_xO_4$ M = Ni, Zn, Co, Mn	Glass	~100[d]	Spinel	None	6.6	3,000–6,000	n.r.	[238]
Fe_3O_4	Glass	~100[e]	Spinel	None	6.9	39,600	5,000	[239]
$Fe_2O_{3-\delta}$	Alumina, Ti	97[e]	Spinel	None	11–13	9,960	5,000	[241]
Ba-Fe-oxide	Alumina, Ti	97[e]	Spinel (Ba/Fe>0.06: amorphous)	Optional	11–13	180–9,960	5,000	[241]
Y-Fe-oxide	Quartz, PET[b]	70–95[e]	Amorphous	650	5.8–8.0	90–360	2,000	[243]
$Fe_{3-x}O_4$	Glass	85[f]	Spinel	None	5.0–7.0	90–460	460	[244]
$Ni_xZn_yFe_{3-x-y}O_4$	Glass	85[f]	Spinel	None	Basic	700	350	[245]
$(Fe_3O_4)_{1-x}(\gamma - Fe_2O_3)_x$	Glass	24[g]	Spinel	None	7.7–8.8	36–380	1,100	[228, 247]

[a]Films prepared by spin spray, spin drip or hydrothermal method are not included.
[b]PET: polyethylene terephthalate, PTFE: polytetrafluoroethylene.
[c]LFD technique (see also Table 7).
[d]"Light-enhanced ferrite plating" (in LFD technique).
[e]"Laser-enhanced ferrite plating" (in LFD technique).
[f]"Ultrasound-enhanced ferrite plating" (in LFD technique).
[g]"Room-temperature ferrite plating" (in LFD technique).

e.g., between Fe and Mn, Ba, and Ni. Therefore in later work [241, 242], a chelating agent (tartrate anion, $C_4H_4O_6^{2-}$) was used to form metal-tartrate complexes at high pH (11–13)—another similarity to CBD. (In these experiments, the researchers used the liquid flow technique with "light enhancement".) From solutions of iron chloride, sodium potassium tartrate, and sodium hydroxide (for control of pH), the as-deposited films were unoriented crystalline spinels which exhibited magnetic hysteresis but no preferred axis of magnetic orientation. From mixed Ba-Fe chloride solutions, Ba tended to deposit more readily than Fe (i.e., the ratio of Ba to Fe in the film was greater than that in the solution). The films with Ba/Fe of ~0.1 were amorphous as deposited, but they contained barium hexaferrite ($BaFe_{12}O_{19}$) as the only crystalline phase after heat treatment at 800°C in air for 10 h.

The actual growth rates still depend strongly on the chemistry of the particular metal cations. Xe-lamp irradiation of mixed Fe-Y chloride solutions [243] achieved growth rates of at most 6 nm min^{-1}. Other significant features of these films were their ferromagnetic behavior (albeit weak) at room temperature, even though they were amorphous in XRD; the strong Y excess (by a factor of 6) needed in the solution to obtain films with the desired stoichiometry (i.e., that of $Y_3Fe_5O_{12}$, yttrium iron garnet); and that they crystallized to the garnet phase on heating to 650°C or above in air.

Magnetite [244] and $Ni_xZn_yFe_{3-x-y}O_4$ films [245] with improved microstructure have been deposited by applying ultrasonic waves of 19.5 kHz and 600 W in continuous flow technique. "Ultrasound-enhanced" ferrite plating was originally developed to encapsulate polymer microspheres (<0.3 μm in diameter), which became discontinuously or insularly coated without applying ultrasound [246]. Sonochemical reactions (e.g., OH group formation on the substrate) are suggested to be responsible for the improved microstructure, and for the increased Ni content in the NiZn ferrite films.

Ferrite plating at room temperature (versus 55–100°C previously) was recently demonstrated [247]. In this approach, a cylindrical glass apparatus was used, with inlets for $FeCl_2$ and basic $NaNO_2$ solution at the bottom. Glass plates as substrates were rotated by magnetic stirrers attached to their back sides. Compared to the previous work, the pH of the mixed solution was higher, due to the shift of the Fe^{2+}/Fe_3O_4 equilibrium to higher pH at lower temperature. Single phase, polycrystalline spinel films without preferred crystallographic orientation were formed with growth rates of 0.6–6.3 nm min^{-1}.

Multilayers of magnetite and CdS were deposited using alternating flowing liquid precursors from the FP and CBD techniques [248]. The thickness of the CdS layers was fixed at 100 nm (growth rate of 3 nm min^{-1}), whereas the thickness of the ferrite layers was controlled at either 32, 80, or 160 nm (5 nm min^{-1}). While the thicker magnetite layers exhibited saturation magnetization nearly equal to that of bulk materials, this property decreased as the thickness of the magnetite layers decreased.

Nagata and Iwahara [249] adapted the ferrite plating concept to deposit films of Mn_2O_3 and a precursor to the SOFC cathode material $La_{1-x}Sr_xMnO_3$. They used hydrogen peroxide as an oxidizing agent, which was added to the solution of Mn(II) just before dripping it onto an yttria-stabilized zirconia substrate. Etching of the substrate, and utilization of a 2-step catalytic treatment prior to deposition, had no effect on the growth rate of the film. This led them to conclude that the operative mechanism of deposition was different from that of electroless plating. Multiphase films containing crystalline Mn_2O_3 were deposited from appropriate solutions of Mn(II) nitrate. The La-Sr-Mn films gave no crystalline XRD pattern as deposited, but developed a multiphase structure (including the desired perovskite) on firing at 1000°C in air. As with most attempts to deposit multicomponent films, the stoichiometry of their films varied from that of the starting solution, in this case being deficient in La and Sr.

3.4. Use of Functionalized Surfaces

3.4.1. Introductory remarks. A significant recent trend in research on low-temperature deposition of thin films has been the use of organic modifications of inorganic surfaces to promote the formation of films from liquid media. Much of the inspiration for such research comes from the field of biomineralization. Living organisms use organic surfaces (such as protein or phospholipid layers) to produce certain inorganic materials (e.g., apatite and the polymorphs of calcium carbonate) with highly controlled microstructures [250, 251] and enhanced physical properties [252]. Researchers have attempted to adapt some of the key features of these processes to the production of films for electronic, optical, and magnetic applications (reviewed here), as well as for biomedical, mechanical, chemical, and thermal applications [253, 254].

3.4.2. Examples of films on SAMs. The earliest attempts to use organic surfaces to influence the formation of synthetic inorganic oxides involved direct precipitation of crystalline SiO_2, TiO_2, iron oxides, and silver oxide within polymer matrices. This work was summarized by Calvert and Mann [255]. Typically, these polymer-ceramic composites consisted of oxide particles, 10–30 nm in diameter, often in clusters up to 5 μm in diameter.

More recently, specifically with a view toward forming thin films, organic self-assembled monolayers (SAMs) have been used to tailor the chemical characteristics of substrate surfaces. SAMs are ultrathin layers (typically 2.5 nm or less) formed via the spontaneous attachment of hydrocarbon molecules onto a substrate, comprising structurally ordered, two-dimensional arrays [256, 257]. One end of each surfactant molecule bonds to the substrate: thiol groups ($-$SH) bond to noble metals such as Au, while trichlorosilane groups ($-SiCl_3$), after hydrolysis to silanol ($-Si(OH)_3$), bond to surfaces such as glass, sapphire, and the native oxides on Si, Ge, and Ti. The functional group at the opposite end of the molecule (or a group that replaces it in a post-deposition displacement or transformation) determines the surface chemistry of the SAM, whether acidic or basic, hydrophilic or hydrophobic, polar or non-polar.

Table 7 summarizes reports on the use of SAMs to promote the deposition of oxide films. In general, the chemistry used to induce formation of the inorganic solid in these cases resembles that of CBD, with control of temperature and pH (and metal concentration to a lesser extent) being the primary means for controlling the rate of film growth.

Rieke et al. [117, 258, 259] deposited goethite (α-FeOOH) films from iron (III) nitrate solutions and akaganeite (β-FeOOH) films from iron (III) chloride solutions onto sulfonate ($-SO_3H$)-terminated SAMs and sulfonated polystyrene. (Maiti et al. [260] observed the same dependence of polymorph on counteranion.) To avoid bulk precipitation for times up to 6 h, they carefully controlled the pH at 2.0–2.1, the [Fe] at 1–3 mM, and the temperature at 70°C. In the absence of bulk precipitation, dense polycrystalline films up to 1.0 μm thick formed that exhibited preferred orientation ([020] axes perpendicular to the substrate). Films formed more quickly (shorter induction times and faster growth rates) at higher degrees of supersaturation (i.e., pH up to 2.57 for the same metal concentrations), but bulk precipitation also occurred sooner, depleting the solution of metal and effectively shutting off the growth of the film. Films that formed while bulk precipitation was taking place were reported to be discontinuous, less dense, and less adherent than films formed exclusively via heterogeneous nucleation.

Nagtegaal et al. [284, 311] used thiol-anchored SAMs on gold as surfaces for deposition of iron oxyhydroxide films. Their solutions (2 mM Fe(III) nitrate, room temperature, pH = 2.86) were maintained below supersaturation; raising the pH to 3.48 led to bulk precipitation and a suppression of film formation. The films contained γ-FeOOH (lepidocrocite), a different polymorph than Rieke observed. Films were observed to form on sulfonate-SAMs, on gold, and on uncoated glass substrates, but not on alcohol-, methyl-, carboxylate-, phosphonate-, or amine hydrochloride-terminated surfaces. They attributed this specificity to the ability of the sulfonate group, alone among the functionalities studied, to deprotonate even in acidic environments, binding positively charged iron ions or complexes from the solution. FTIR spectra gave evidence for such an interaction.

Koumoto et al. [289] deposited TiO_2 (anatase) from an LPD-type solution (after Deki et al. [60]). The anatase was preferentially oriented with the *c*-axis perpendicular to the substrate surface. This alignment led them to conclude that heterogeneous nucleation was the dominant mode of formation of these films, with the nucleation sites being Si-OH groups on the surfaces.

The present authors and their co-workers have used SAMs to synthesize films of several oxides (Table 7). Crystalline films of TiO_2 [261–264], ZrO_2 [264–267], FeOOH [268], AlOOH [269] and SnO_2 [270–272] were formed directly from aqueous solutions below 100°C. Films of ZnO [273], Y_2O_3 [274], $ZrTiO_4$ [275], Y_2O_3-ZrO_2 [265], V_2O_5 [276], and Fe_3O_4 [268] were formed after moderate heat treatments. Typical films were $<$100 nm thick, with crystals 2–10 nm in diameter in a small amount of non-crystalline matrix. Significant exceptions were the FeOOH films, which frequently exceeded 100 nm in thickness, and the Y- and V-containing films, which were amorphous before heat treatment.

Niesen et al. [264] have studied the topography of these films using AFM. The smoothest regions of these films exhibit roughness values ranging from 1 to 4 nm, somewhat rougher than either the SAMs or the oxidized silicon substrates. The film surfaces appear to be made up of well-packed agglomerates of nanocrystals a few nanometers in size. The agglomerates have diameters

Table 7. Oxide and sulfide thin films deposited on self-assembled monolayers.

System			Temperature (°C)			pH	Growth rate (nm h^{-1})	Max. thickness (nm)	Reference
Oxide	Functional group	Substrate	Deposition	As-deposited	Annealing				
Y_2O_3	$-SO_3H$	SiO_2/Si	80	Amorphous	600	4–6.5	~2	35	[274]
TiO_2	$-SO_3H$	SiO_2/Si	80	Anatase	200–600	Acidic	~25	50	[261–264]
TiO_2	$-SO_3H$	Glass	80	Anatase	None	Acidic	~30	~60	[307–310]
TiO_2	$-SO_3H$	SiO_2/Si, glass	22–90	TiO_2 (B)	None	1.5–2.5	10–3000	>150	[281]
TiO_2	$-SO_3H$	SiO_2/Si	70–80	Anatase	None	0.8–1.0	5–45	170	[276, 282]
TiO_2	Phenyl	SiO_2/Si	50	Anatase	None	2.88	n.r.	n.r.	[289]
ZrO_2	$-SO_3H$	SiO_2/Si, glass, sapphire, SiC	70	Tetragonal ZrO_2	500	Acidic	1–25	125	[264–267]
Y_2O_3-ZrO_2	$-SO_3H$	SiO_2/Si	80	Amorphous	500–800	2.2–6.5	~3	25	[265]
V_2O_5	$-NH_2$	SiO_2/Si	45	$V_2O_5 \cdot H_2O$	350	~1.3	1–4	90	[276]
α-Fe_2O_3; Fe_3O_4	$-SO_3H$	SiO_2/Si	100	β-FeOOH	300, air + 500, vac.	<1.2	150	150	[268]
α-FeOOH β-FeOOH	$-SO_3H$	SiO_2/Si	70	α-FeOOH β-FeOOH	None	2–3	1–22	1000	[117, 258, 259]
γ-FeOOH	$-SO_3H$	Au	20	γ-FeOOH	None	2.86	<1	11	[284, 311]
Fe_3O_4	—OH	Au on Si	70	Spinel	None	7	n.r.	n.r.	[291]
ZnO	$-SO_3H$	SiO_2/Si	35	$Zn(OH)_2$	400	11	~20	9[a]	[273]
ZnO	$-NH_2$	SiO_2/Si	20	ZnO_x	n.r.	Basic	[b]	13	[280]
SnO_2	$-SO_3H$	SiO_2/Si	80	Cassiterite	None	1.3–1.5	3–10	50 (1×) 82 (2×)	[270–272]
PbS	—COOH	Au on glass	25	Galena + amorphous	None	~13	3–10 (after incubation)	>300	[118]
CdS	$-CH_3$	SiO_2/Si	35–75	Cubic + hexagonal CdS	None	10.5–10.7	n.r.	290	[292]
ZnS	—COOH	Au on glass	25	n.r.	None	Basic	0.2–0.3 nm/cycle	n.r.	[277]

[a]After annealing.
[b]SILAR technique, 24.5 nm/cycle.

of up to about 100 nm (Fig. 4(a)). On the micron scale, protrusions and depressions can be observed in the films, sometimes isolated and sometimes in patches a few square microns in extent. These features range up to 50 nm in depth/height and are typically 0.5–1 μm in width (Fig. 4(b)). Whereas the origin of the nanoscale roughness appears to be the crystallite size (as observed in TEM images of these films), the micron-scale features may be related to the attachment and detachment of large agglomerates, and possibly to imperfections (pinholes; adsorbed contamination) in the SAM. Similar conclusions were drawn from SEM studies of the films [267].

Meldrum et al. [118, 277, 278] investigated the growth of sulfide thin films on self-assembled monolayers on gold, using surface plasmon spectroscopy (in situ) and microscopic techniques (ex situ). PbS films were formed by CBD from alkaline $Pb(ClO_4)_2$ solution and thiourea at room temperature, and the influence of the monolayer terminal group on crystal growth was investigated for $-$COOH, $-$OH, $-NH_2$, $-SO_3H$ and $-CH_3$ functionalities [118, 278]. If 2 M NaOH was used, films deposited most readily on SAMs bearing terminal groups with high dissociation constants (i.e., $-$COOH and $-SO_3H$), while $-$OH, $-NH_2$, and $-CH_3$ surfaces did not provide good growth substrates. (Note that films were also formed directly on the bare gold substrate.) The observed induction period for film growth was attributed to the slow formation and adsorption of amorphous $Pb(OH)_2$ particles, followed by conversion into PbS crystallites of 5–10 nm in size. Further growth by an ion-by-ion mechanism could explain the alteration of the crystal size (20–30 nm in diameter) experimentally found after film thickness exceeded 25 nm. From 5 M NaOH, films could be deposited on *all* substrates. Here, film growth seems to start from particles of diameter on the order of 20 nm. This was related to the fact that increasing the concentration of NaOH favors the formation of the (soluble) anion $HPbO_2^-$, suppressing the primary particle formation mechanism and promoting the slower, but less surface-specific ion-by-ion growth. No geometrical match at the substrate/crystal interface was required to reach crystal orientation; on the contrary, SAMs from short chain surfactants (i.e., those which are less ordered) and the bare gold substrate itself led to the highest degree of orientation.

ZnS thin films [277] were formed by SILAR, i.e., alternate immersions of the substrates in zinc nitrate and sodium sulfide solution. On $-$COOH terminated SAMs, films were formed of a uniform distribution of spherical particles of $\sim$20 nm in diameter. Surface plasmon spectroscopy revealed a growth rate of 0.2–0.3 nm/cycle, which is in agreement with earlier results on glass substrates (see § 2.2.2). If patterned substrates (see below) were used [279], deposition seemed to be restricted to the hydrophilic ($-$COOH) areas, consistent with the SILAR deposition mechanism.

ZnO films [280], also deposited by the SILAR technique, could be selectively formed on amine-modified silicon wafers while bare silicon remained unreactive under the same conditions. (Note that other groups have reported SILAR of ZnO films without substrate functionalization, see § 2.2.4). The films consisted of extended islands (50–500 nm), which was mainly related to the patchy organic monolayer resulting from the short-chain hydrocarbons used. To explain the smoothness of the islands, lateral mobility of small clusters on the disordered amine surface was assumed.

3.4.3. Discussion. In most of the studies reviewed in this section, the solutions were acidic and, in contrast to CBD of sulfide films, no complexants were used. Two exceptions were the work of Baskaran et al. [281] and Niesen et al. [276, 282]. Baskaran et al. used a lactate complex of Ti as their metal precursor. The resulting additional stability against precipitation allowed them to work at much more moderate pH (1.5–2.5; Table 7) than did Shin et al. [261] (who used 6 M HCl). Niesen's approach was to complex Ti with hydrogen peroxide, which served a similar function. These studies clearly show that the use of complexants, well developed in the CBD literature, can provide a useful additional means of controlling the deposition of metal oxides, especially with regard to the time needed for nucleation and growth of the solid at a given pH or metal concentration.

The CBD literature on sulfide films also sheds light on the mechanism of growth of oxide films. In both cases, the mode of growth (ion-by-ion vs. particle attachment) cannot be unambiguously ascertained by an examination of the microstructure, but certain guidelines appear valid. Crystallographic orientation in polycrystalline films argues strongly that heterogeneous nucleation occurred, followed by ion-by-ion growth. As proposed by Gorer and Hodes [102], films with crystals larger than about 16 nm probably formed by ion-by-ion growth. Both of these criteria are consistent with the conclusions of Rieke et al. [117, 258], whose oriented FeOOH films had crystals 30–50 nm in size.

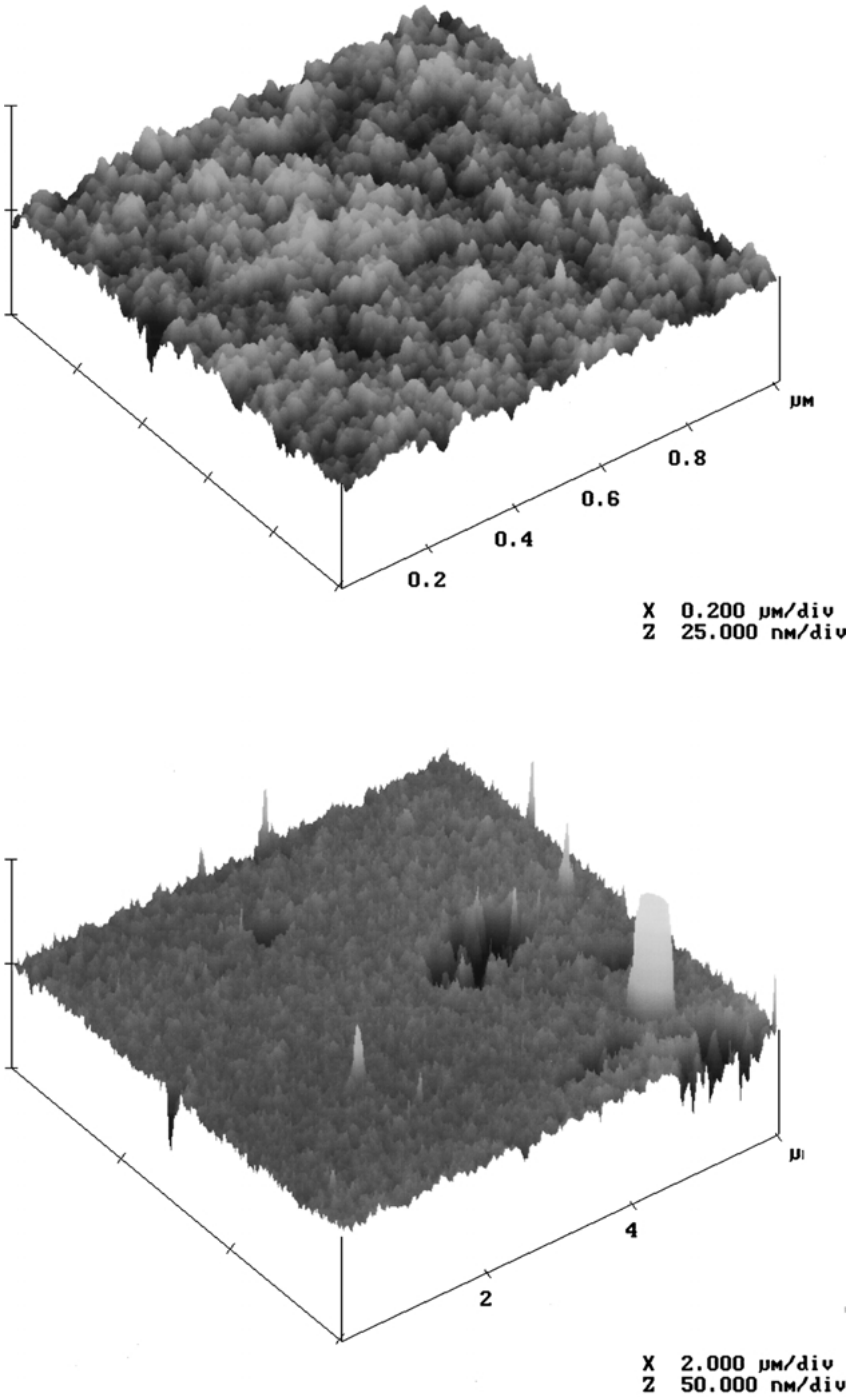

Fig. 4. AFM images of a nanocrystalline zirconia film deposited on a sulfonate SAM. Deposition conditions: 4mM $Zr(SO_4)_2$, 0.4 M HCl, 70°C, 4 consecutive 1-hour immersions. a) 1 μm × 1 μm area, showing nano-scale roughness. (Horizontal scale: 0.2 μm div^{-1}; vertical scale: 25 nm div^{-1}.) b) 6 μm × 6 μm area, showing micron-scale roughness. (Horizontal scale: 2 μm div^{-1}; vertical scale: 50 nm div^{-1}.)

In contrast, the films reported by De Guire et al. usually contained crystals smaller than 10 nm, and their growth conditions and morphologies were consistent with particle attachment. They proposed [283] that forces similar to those that exist between colloidal particles in fluids could lead to film growth. Derjaguin-Landau-Verwey-Overbeek (DLVO) theory provided a means to estimate the magnitude of these forces. Their calculations are in agreement with several experimental observations. For example, only particles ~2–10 nm in size should form films. The calculations also predict the observed lack of deposition of ZrO_2 films on SAM-free silicon [283] and differences in SnO_2 films between SAM-coated and SAM-free substrates [272]. However, they could not account for the observed specificity of TiO_2 to deposit on sulfonate but not on thioacetate SAMs.

Several considerations must be kept in mind when applying DLVO theory to such systems. First, the length scales are much smaller than in typical colloidal systems: the particles are nanometers, rather than microns, in size, and the calculated Debye layers can be very thin (<1 nm), a result of the solutions' comparatively high concentrations compared to the dilute electrolytes usually considered. The applicability of DLVO calculations becomes less certain as these lengths approach the size of the complexes in the solution. Furthermore, unlike typical powder suspensions in which the surrounding fluid is chemically inert with respect to the solid, the particles forming films here are in continuous reaction with the liquid media, even after (and if) they deposit on a substrate. The particles' extremely high surface-to-volume ratio might lead to a kind of liquid-phase sintering despite the relatively low temperatures, leading to denser microstructures than are typical of systems dominated by DLVO-type interactions.

One of the interactions treated explicitly in the DLVO calculations is the electrostatic interaction between particles and the substrate. This focuses attention on two factors: the surface charge density of the SAM, and the charge on the particles (which depends on their isoelectric point in comparison to the pH of the deposition medium). Empirically, the sulfonate SAM has been shown to be an especially versatile surface for oxide deposition (Table 7). This appears to be linked to its unique capability among the surfaces studied to deprotonate (and therefore to become negatively charged) even in acidic environments [283, 284] where most oxide particles are positively charged. The work on V_2O_5 films by Niesen et al. [276] represents an important test of this hypothesis, because V_2O_5 is negatively charged in the solutions from which it was deposited (pH of 1–4). It was found not to deposit on sulfonate SAMs, but did deposit on amine SAMs, which will be positively charged at this pH. This provides convincing, if qualitative, support for the key role played by the uniform, concentrated surface charge density of hydrophilic SAMs in promoting growth of oxide films.

This group has studied the chemical limits of silanol-anchored SAMs and how these limits affect the processing of thin films on SAMs. The silanol linkage is highly resistant to acidic media even at elevated temperatures (<100°C). In contrast, basic media are known to attack the Si-O-substrate bonds. Therefore, the use of these SAMs for film deposition is limited to oxides that will precipitate under neutral or acidic conditions, i.e., small, highly-charged cations such as Ti, Zr, Sn, and Y. For deposition of ZnO films under basic conditions, silane-anchored SAMs met with more limited success [273]. Correspondingly, deposition of oxides of alkali or alkaline earth metals, Pb, and other large monovalent or divalent metals would require a SAM that could better withstand basic environments. Compound oxides of mixed acidic and basic character (e.g., $BaTiO_3$, $LiNbO_3$) could probably best be approached via hydrolysis of non-aqueous media.

Heat treatment of the oxide deposits on SAMs leads to the pyrolysis of the organic layer. Wang et al. [269] studied the thermal decomposition of silanol-anchored SAMs with and without overlying oxide films. The organic film burned off completely within 2 h at temperatures between 200 and 400°C, as shown by TEM, surface chemical analysis, and thermogravimetry. Recent results of Ritley et al. [285] using in-situ x-ray reflectivity have also shown that the SAM breaks down above 300°C. (Kluth et al. [286] reported that such SAMs are stable to temperatures of at least 467°C, but their samples were heated for only 1 minute.) This pyrolysis (somewhat unexpectedly) does not disrupt the adhesion of the inorganic overlayer [261, 264, 265, 274]. It is believed that the hydrocarbon combustion products can diffuse through small channels several Ångstroms wide that open up between some of the nanocrystals upon crystallization of the amorphous matrix, allowing a new oxide-substrate interface to form. In this regard, it should be pointed out that the total amount of the combustion products is extremely small (nanomoles per square centimeter) so that pyrolysis of the SAM under even a relatively thick film (e.g., 1 μm)

is not expected to diminish the adhesion of the oxide layer.

3.4.4. Patterning of films on SAMs. Several techniques for producing patterned SAMs, and for using them to produce patterned ceramic thin films, have been reported. All of these approaches have relied on the general preference for oxides or sulfides from aqueous solutions to deposit onto hydrophilic surfaces and not onto hydrophobic surfaces. Rieke et al. [287, 288] rastered electron and ion beams across a methyl-terminated SAM on Si, then deposited vinyl-terminated surfactant selectively with 1–3 μm resolution where the hydrophobic methyl SAM had been removed. The vinyl-functionalized regions were then converted to hydrophilic sulfonate by exposure to SO_3 vapor, after which FeOOH was deposited (see above) with resolution of 10–15 μm. One disadvantage of this technique is that the time needed to produce a pattern by rastering is relatively high. Collins et al. achieved a bifunctional patterned surface with 10-μm features in a single step, shining UV light through a mask to convert a moderately hydrophobic thioacetate SAM on Si selectively to sulfonate [262]. Anatase (TiO_2) was then deposited from a $TiCl_4$/HCl solution. Meldrum et al. photooxidized thiol-anchored SAMs of hydrophilic 16-mercaptohexadecanoic acid on Au and readsorbed 16-mercaptohexadecane [279], then deposited PbS as described above. The work of Koumoto et al. on anatase films [289], described earlier, used a similar approach with silanol-anchored SAMs on Si, using UV light to cleave hydrophobic phenyl surface groups. Features as small as 15 μm were clearly developed in the anatase film.

These approaches offer the potential of obtaining patterned films without the use of photoresists and strippers. Most of these techniques can be used to deposit either a "positive" or a "negative" image, depending on the affinity or aversion of the film for the various types of SAMs and substrates. While successful as proofs of concept, these studies showed that more work is needed to achieve feature sizes smaller than several microns. The resolution appeared to be limited by the oxide deposition rather than by the patterning of the SAM. In each case dense, adherent films deposited on the hydrophilic regions, but thin layers or dispersed precipitates were observed on the hydrophobic regions. Even when such deposits do not adhere strongly to the substrate, they may bridge across to the hydrophilic regions, with interactions at least as strong as those that keep the film itself intact [283]. Tearing of these interparticle bonds during removal of the unintended deposit probably led to the ragged feature edge observed by Koumoto et al. and to unacceptably high variations (28%) in feature width for electronic applications [289]. Therefore, to make this approach practical, it may be important to avoid deposition on the hydrophobic areas more completely via optimization of the deposition time and conditions.

A technique for selective initial placement of the SAM itself called microcontact printing was developed by Kumar and Whitesides [290]. As with inking of a rubber stamp, a molded elastomer template is dipped in the surfactant solution, then pressed against a substrate to transfer the surfactant to it. The un-stamped areas can subsequently be filled in with a SAM of complementary functionality by simple immersion in the appropriate surfactant solution. Although limited by the resolution of the stamp and the mechanical stability of the process, it is a fast, inexpensive, and versatile approach that can be readily adapted to a rapid manufacturing setting. Patterned deposition of ferrite (using liquid-flow ferrite plating, § 3.3 and § 3.5) with features about 1 μm in size and good resolution was demonstrated [291]: The films were formed on areas functionalized with —OH groups while areas functionalized with —SH were resistant to deposition. In the case of CdS film formation (by CBD, § 2.1), under optimized conditions, selective deposition on SAM-free regions could be achieved while areas with —CH3 functionalization remained film-free [292]. However, such films often showed small CdS islands on the SAM and holes in the CdS film. Better resolution was achieved when a continuous CdS film was formed first on the entire surface, followed by lift-off sonication, which removes the film from the SAM-coated areas. The roughness of the boundary between the CdS layer and the OTS-protected region was reported to be in the range of <100 nm.

3.4.5. Multilayer and higher-order structures. The use of organic surfaces offers the potential to develop materials and structures with applications beyond the scope of the present review, e.g., organic-inorganic composites with hierarchical structures exhibiting organization on one or more length scales. For example, Kotov et al. [293] built up alternating multilayer sequences of polyelectrolyte-(CdS particles)-polyelectrolyte-(TiO_2 particles) tens of layers thick on noble metal, glass, mica, and Teflon substrates. They studied the dependence of the photocurrent on

the layer sequence and dimensions of their films. Liu et al. [294] similarly built up polyelectrolyte-TiO_2 multilayers and characterized their UV-visible transmission. While these two studies used the organic layer to assemble pre-existing inorganic particles, Aksay et al. [295] used micellar assemblies of surfactant molecules and inorganic precursors, spontaneously formed in solution, to create silica films that exhibited various types of structural order on the nanometer scale.

3.5. Liquid Flow Deposition (LFD)

3.5.1. General remarks. During deposition of a solid film from a static liquid, such as those used in CBD or LPD as described above, gradual changes in the composition of the liquid will occur. It will become depleted of the metal and anion, as the solid reaction product deposits on the substrate or simply precipitates from solution. Film growth slows down and eventually stops. In addition, any thermally decomposing reagent and its byproducts, such as urea forming ammonia and carbon dioxide in certain CBD processes, will exhibit time-dependent concentrations which will further affect the deposition rate. Although these changes can be readily predicted and controlled, they impose limitations on the maximum achievable growth rates and film thicknesses.

In liquid flow deposition (LFD), the deposition medium is continuously flowed (usually by means of a pump) past the substrate. The reactants in the deposition medium are replenished continuously. While the temperature and composition of the solution can still be used to control the rate of reaction, the rate of flow of the deposition medium past the substrate becomes a new and easily controlled variable for adjusting the deposition process. With proper design of the reaction chamber and tailoring of the flow rate to the reaction kinetics, a steady state can be achieved which exposes the substrate to a medium of constant composition and reactivity. In several cases, constant and high growth rates have been achieved with no evidence of slowing down at longer times, implying no limitation on the maximum achievable film thickness. Alternatively, the process can in principle be designed to vary the composition, growth rate, and microstructure even within a single film, though this strategy for producing graded films apparently has yet to be exploited.

The techniques discussed previously have been categorized in chemical terms: pH ranges, use of complexants, redox reactions, etc. In contrast, the concept of LFD can be applied to any of the main techniques described so far (with the possible exception of SILAR) without changing the basic chemical reactions involved in forming the film. Therefore, we describe it here as a variation of these techniques, while recognizing that it offers a wealth of new options for control of the deposition process that are not possible with static deposition media. Table 8 presents a summary of work on LFD of oxide films.

3.5.2. LFD of oxide and sulfide films. In the late 80's, Goto et al. [233, 234] reported a modification of the ferrite plating process in which two separate aqueous solutions (one containing $FeCl_2$ and ammonium acetate (CH_3COONH_4), the other containing sodium nitrite ($NaNO_2$) and ammonium acetate) were combined and flowed as a shallow confined liquid stream past a glass substrate (§ 3.3).

Ito and co-workers [296, 297] used this design to deposit CdS films from a buffered ($7.5 < pH < 9.0$), combined aqueous solution of $CdCl_2$ and H_2S at 40–80°C. Their chemistry resembles that of a CBD process, with

Table 8. Oxide thin films deposited via liquid flow deposition (LFD).

System		Temperature (°C)						
Oxide	Substrate	Deposition	As-deposited	Annealing	pH	Growth rate (nm h^{-1})	Max. thickness (nm)	Reference
Fe_3O_4, $Co_xFe_{3-x}O_4$	Glass, sapphire, spinel, PET,[c] PTFE[b]	55–90[a]	Spinel	None	6.9–7.3	960–2,400	800	[233, 234, 305, 306]
ZnO	Glass	70	ZnO	None	8.0	600	1000	[302]
SnO_2	Si	80	SnO_2	None	Acidic	65	1000	[270, 271]

[a]LFD technique (see also Table 7).
[b]Polytetrafluoroethylene.
[c]Polyethylene terephthalate.

adjustment of the flow rate providing an additional means of controlling the rate of reaction. Regardless of the cadmium salt used (chloride, sulfate, nitrate, or acetate), their films were single-phase hexagonal CdS, with the *c*-axis predominantly perpendicular to the substrate. The minimum film resistivities (4–20 Ω cm, potentially acceptable for heterojunction solar cells with $CuInSe_2$) were achieved at 60°C, pH = 8.0, and flow rates of 0.2 mL min^{-1}, which yielded deposition rates of 10 nm min^{-1} and films 30 nm to 1 μm thick.

Oladeji et al. [298, 299], taking into account the saturation of a static deposition, *periodically* replenished their CdS deposition solution, consisting of cadmium acetate, thiourea and ammonia/ammonium acetate buffer at 85°C, in cycle periods of 30–90 min. Polycrystalline films (cubic CdS) with thicknesses between 0.13 and 0.6 μm were formed and a thickness yield of 42–47% per cycle relative to that obtained in the initial deposition cycle was found.

Boyle et al. [300, 301] suggested keeping the CdS deposition solution at room temperature and to heat the substrate directly to 80°C, while recirculating and filtering the deposition solution and replenishing the reagents in a closed-loop CBD reactor. The advantage of this process is the significant reduction of the amount of (cadmium) waste. The authors used a deposition solution containing $CdCl_2$, ethylenediamine, thiourea and NaOH (pH = 12.5). As-deposited films were composed of mixed cubic and hexagonal phases, in the form of dense, asymmetric grains each 50–100 nm in diameter. Annealing in air at 400°C effected conversion to hexagonal CdS without significant grain growth.

Ito and Nakamura [302], with a view towards gas sensors and electrophotography, adapted the liquid-flow concept also to ZnO. Their solution consisted of aqueous $ZnCl_2$ and urea (each 10 mM) at 70°C and a constant pH of 8. The films were single-phase, hexagonal, *c*-oriented ZnO as deposited with a resistivity of 0.1 Ω cm. They grew at 10 nm min^{-1} to a thickness of 1 μm and could not be removed with a finger-scratch.

Supothina and co-workers [270, 271] reported the first systematic study of the effect of flow rate and chamber configuration on the growth rate of LFD films. They deposited nanocrystalline α-SnO_2 (cassiterite) on silicon (100) substrates with and without sulfonate-functionalized self-assembled organic monolayers. The films, deposited from acidic $SnCl_4$/HCl solutions at 80°C, consisted of randomly oriented crystals 5–10 nm in diameter. Their work showed that, for a given solution and chamber configuration, the flow rate can be optimized to give the maximum growth rate by tailoring the average residence time of the solution in the chamber to the time required for the first appearance of visible precipitation. Their maximum growth rates were 1.0–1.3 nm min^{-1} (depending on the degree of supersaturation of the solution) and the maximum thickness achieved was 1.0 μm.

4. Summary and Concluding Remarks

Numerous oxides have been produced as polycrystalline thin films from aqueous solutions at low temperatures. Typical film thicknesses range from a few nanometers to about one micron. Growth rates are usually a few to a few hundred nanometers per hour, but rates of microns per hour have been reported. The particle sizes in the films range from a few nanometers to a few tens of nanometers. All described techniques, with the notable exception of SILAR, start in principle from a single bath containing cation and anion sources.

Although most of the examples reported to date are single oxides, multicomponent films have been deposited, including doped single oxides (ZnO:Ni, Cu, Cd, Al, Sn; SnO_2:Sb; In_2O_3:Sn) solid solutions (spinel ferrites; ZrO_2-Y_2O_3), and stoichiometric compounds ($CdSnO_4$; perovskites). From a practical point of view, the relative metal concentrations in solutions must be adjusted empirically to obtain a desired ratio of metals in the film; different precipitation kinetics can make it difficult to achieve simultaneous and uniform precipitation of both components in the ratios desired for stoichiometric mixed oxides. Usually, oxides of the higher-valent (III–V) metals can be deposited as films from acidic solutions, whereas lower-valent (II–III) metals have been deposited at neutral to basic pH. This reflects a fundamental difference in the precipitation chemistry of these metals, and affects the ability of forming multicomponent films. Some of these difficulties may be solvable through reference to the extensive literature on deposition of non-oxide films from aqueous solutions, or to the sol-gel literature where films of such mixed-oxide compounds as Pb(Zr, Ti)O_3, $BaTiO_3$ and $LiNbO_3$ have been successfully synthesized. The SILAR technique, with its advantage of easier incorporation of dopants, seems to be limited by the step-by-step processing and the resulting low growth rate. Lastly, we note that residual anions from the solution are frequently included films formed via these liquid-deposition techniques; these can be desirable or undesirable, depending on the application.

The much larger body of work on liquid-phase synthesis of sulfides and selenides also sheds light on the mechanisms by which the oxide films form. In both cases, chemical control (pH, temperature, metal concentrations) determines the rate of solid formation. In general, increasing the degree of superaturation through chemical means raises the growth rate but limits the final thickness of the films. On the other hand, the substrates (e.g., through the use of functionalized surfaces) and the design of the reaction chamber (e.g., in liquid flow deposition) influence the location of nucleation and the rate of growth. Control of the relative rates of ion-by-ion growth and particle formation/attachment is needed to avoid the formation of non-adherent, porous, or powdery deposits. The main difference between oxides and non-oxides in this context is that the concentration of the anionic component (S^{2-} or Se^{2-}) in a non-oxide film is a separate adjustable parameter, affording an additional element of control over the film formation process.

Several researchers have espoused the importance of nucleation on the substrate to form good-quality films. Nevertheless, numerous examples have been reviewed here for which bulk precipitation appears to have played a significant role in the growth of dense, adherent films. Clearly it is possible to take advantage of the faster rates of nucleation and/or growth provided by precipitating solutions to obtain useful films (e.g., in LFD). In many cases, only a narrow window of conditions will maintain the metastability needed for purely heterogeneous nucleation. While control of temperature, pH, and bath composition will be crucial for satisfactory results with any of the techniques described here, the use of precipitating solutions may relax some of the constraints and ultimately prove more practical for large-scale production.

Most of the examples reviewed here have used substrates (usually silicon or glass) without special surface functionalization. However, functionalized surfaces have enabled deposition under conditions where it would not otherwise have occurred. Among these surfaces, sulfonate self-assembled monolayers (SAMs) have shown a unique versatility for deposition of a variety of oxide and sulfide thin films. Furthermore, functionalized surfaces offer the possibility of patterned deposition (as does photo-assisted deposition).

While liquid-phase deposition offers the capability of depositing films on non-planar surfaces, this has not yet been widely exploited. Potential applications include trench-filling in microelectronics [198] and coatings on powders [269], catalyst supports, fuel cell electrodes, porous capacitors, and battery structures.

More work needs to be done to characterize the properties of these films and to evaluate their suitability for applications. To this end, it is hoped that this review has provided directions along which routes for synthesis of materials with improved microstructures (and thus properties) can be developed.

Acknowledgments

The authors gratefully acknowledge support from the Deutsche Forschungsgemeinschaft (DFG Al 384/22-1/2) and the U.S. National Science Foundation (INT 9726753, DMR 9803851).

Notes

1. Here, "ceramic" refers to polycrystalline inorganic nonmetallic materials, without the additional connotation of high-temperature heat treatment that is usually associated with the term.
2. In those CBD processes that do involve a change in oxidation state of the metal, it usually occurs in the bulk solution prior to formation of the solid.
3. If an oxide film is desired, formation of the hydroxide is in some cases a necessary first step. Even if a non-oxide film is desired, it is believed that hydroxide particles serve as necessary catalysts for the hydrolysis of the chalcogenide source, as discussed in § 2.1.3.

References

1. W.S. Rees (Ed.), *CVD of Nonmetals* (Wiley-VCH, Weinheim, 1996).
2. A.C. Jones and P. O'Brien, *CVD of Compound Semiconductors. Precursor Synthesis, Development and Applications* (Wiley/VCH, Weinheim, 1997).
3. C.J. Brinker and G.W. Scherer, *Sol-Gel Science: The Physics and Chemistry of Sol-Gel Processing* (Academic Press Inc, San Diego, 1990).
4. A.C. Pierre, *Introduction to Sol Gel Processing* (Kluwer Academic Publ., Boston, 1998).
5. F.F. Lange, *Science*, **273**, 903 (1996).
6. F.C. Eze, *J. Phys. D: Appl. Phys.*, **32**, 533 (1999).
7. A.J. Varkey and A.F. Fort, *Solar Energy Mater. Solar Cells*, **31**, 277 (1993).
8. P. Pramanik and S. Bhattacharya, *J. Electrochem. Soc.*, **137**, 3869 (1990).
9. A.J. Varkey and A.F. Fort, *Thin Solid Films*, **235**, 47 (1993).
10. B. Pejova, T. Kocareva, M. Naydoski, and I. Grozdanov, *Appl. Surf. Sci.*, **165**, 271 (2000).
11. A.J. Varkey and A.F. Fort, *Solar Energy Mater. Solar Cells*, **29**, 253 (1993).
12. R.L. Call, N.K. Jaber, K. Seshan, and J.R. Whyte, *Solar Energy Mater.*, **2**, 373 (1980).

13. D. Raviendra and J.K. Sharma, *J. Appl. Phys.*, **58**, 838 (1985).
14. T. Saeed and P. O'Brien, *Thin Solid Films*, **271**, 35 (1995).
15. P. O'Brien, T. Saeed, and J. Knowles, *J. Mater. Chem.*, **6**, 1135 (1996).
16. A.J. Varkey, *Int. J. Mater. Prod. Technol.*, **10**, 94 (1995).
17. A. Ennaoui, M. Weber, R. Scheer, and H.J. Lewerenz, *Solar Energy Mater. Solar Cells*, **54**, 277 (1998).
18. M.Z. Najdoski, I.S. Grozdanov, and B. Minceva-Sukarova, *J. Mater. Chem.*, **6**, 761 (1996).
19. M. Ocampo, A.M. Fernandez, and P.J. Sebastian, *Semicond. Sci. Technol.*, **8**, 750 (1993).
20. R.P. Goyal, D. Raviendra, and B.R.K. Gupta, *Phys. Stat. Sol. A*, **87**, 79 (1984).
21. D. Raviendra and J.K. Sharma, *J. Phys. Chem. Solids*, **46**, 945 (1985).
22. C.D. Lokhande, *Mater. Chem. Phys.*, **27**, 1 (1991).
23. I. Grozdanov, *Semicond. Sci. Technol.*, **9**, 1234 (1994).
24. P.K. Nair, M.T.S. Nair, V.M. Garcia, O.L. Arenas, Y. Peña, A. Castillo, I.T. Ayala, O. Gomezdaza, A. Sánchez, J. Campos, H. Hu, R. Suárez, and M.E. Rincón, *Solar Energy Mater. Solar Cells*, **52**, 313 (1998).
25. O. Savadogo, *Solar Energy Mater. Solar Cells*, **52**, 361 (1998).
26. V.P. Tolstoy, I.V. Murin, and A. Reller, *Appl. Surf. Sci.*, **112**, 255 (1997).
27. V.P. Tolstoi, *Russ. J. Appl. Chem.*, **72**, 1326 (1999).
28. E.V. Tolstobrov and V.P. Tolstoi, *Russ. J. Gen. Chem.*, **69**, 856 (1999).
29. M. Ristov, G.J. Sinadinovski, and I. Grozdanov, *Thin Solid Films*, **123**, 63 (1985).
30. M.T.S. Nair, L. Guerrero, O.L. Arenas, and P.K. Nair, *Appl. Surf. Sci.*, **150**, 143 (1999).
31. V.P. Tolstoi and E.V. Molotilkina, *Russ. J. Inorg. Chem.*, **39**, 372 (1994).
32. M. Ristov, G.J. Sinadinovski, I. Grozdanov, and M. Mitreski, *Thin Solid Films*, **149**, 65 (1987).
33. A.E. Jiménez-González and P.K. Nair, *Semicond. Sci. Technol.*, **10**, 1277 (1995).
34. A. Jiménez-González and R. Suárez-Parra, *J. Cryst. Growth*, **167**, 649 (1996).
35. P. Mitra, A.P. Chatterjee, and H.S. Maiti, *J. Mater. Sci. Mater. Electr.*, **9**, 441 (1998).
36. P. Mitra, A.P. Chatterjee, and H.S. Maiti, *Mater. Lett.*, **35**, 33 (1998).
37. A.P. Chatterjee, P. Mitra, and A.K. Mukhopadhyay, *J. Mater. Sci.*, **34**, 4225 (1999).
38. E.V. Tolstobrov and V.P. Tolstoi, *Russ. J. Appl. Chem.*, **68**, 899 (1995).
39. S. Lindroos and M. Leskelä, *Int. J. Inorg. Mater.*, **2**, 197 (2000).
40. A.E. Jiménez-González, *J. Solid State Chem.*, **128**, 176 (1997).
41. V.P. Tolstoi, *Russ. J. Inorg. Chem.*, **40**, 208 (1995).
42. V.P. Tolstoi, *Russ. J. Inorg. Chem.*, **38**, 1063 (1993).
43. V.P. Tolstoy, *Thin Solid Films*, **307**, 10 (1997).
44. V.P. Tolstoy and A.G. Ehrlich, *Thin Solid Films*, **307**, 60 (1997).
45. V.P. Tolstoi and E.V. Molotilkina, *Inorg. Mater.*, **30**, 201 (1994).
46. Y.F. Nicolau, *Appl. Surf. Sci.*, **22/23**, 1061 (1985).
47. S. Lindroos, T. Kanniainen, and M. Leskelä, *Mater. Res. Bull.*, **32**, 1631 (1997).
48. M.P. Valkonen, T. Kanniainen, S. Lindroos, M. Leskelä, and E. Rauhala, *Appl. Surf. Sci.*, **115**, 386 (1997).
49. M.P. Valkonen, S. Lindroos, T. Kanniainen, M. Leskelä, U. Tapper, and E. Kauppinen, *Appl. Surf. Sci.*, **120**, 58 (1997).
50. T. Kanniainen, S. Lindroos, J. Ihanus, and M. Leskelä, *J. Mater. Chem.*, **6**, 161 (1996).
51. S.D. Sartale and C.D. Lokhande, *Indian J. Pure Appl. Phys.*, **38**, 48 (2000).
52. S.D. Sartale and C.D. Lokhande, *Mater. Chem. Phys.*, **65**, 63 (2000).
53. S. Lindroos, A. Arnold, and M. Leskelä, *Appl. Surf. Sci.*, **158**, 75 (2000).
54. B.R. Sankapal, R.S. Mane, and C.D. Lokhande, *Mater. Chem. Phys.*, **63**, 226 (2000).
55. S. Lindroos, Y. Charreire, D. Bonnin, and M. Leskelä, *Mater. Res. Bull.*, **33**, 453 (1998).
56. B.R. Sankapal, R.S. Mane, and C.D. Lokhande, *J. Mater. Sci. Lett.*, **18**, 1453 (1999).
57. L.B. Gulina and V.P. Tolstoi, *Russ. J. Gen. Chem.*, **69**, 1528 (1999).
58. B.R. Sankapal, R.S. Mane, and C.D. Lokhande, *Mater. Chem. Phys.*, **63**, 230 (2000).
59. P.H. Chang, C.T. Huang, and J.S. Shie, *J. Electrochem. Soc.*, **144**, 1144 (1997).
60. S. Deki, Y. Aoi, O. Hiroi, and A. Kajinami, *Chem. Lett.*, **1996**, 433 (1996).
61. S. Deki, Y. Aoi, Y. Asaoka, A. Kajinami, and M. Mizuhata, *J. Mater. Chem.*, **7**, 733 (1997).
62. S. Deki and Y. Aoi, *J. Mater. Res.*, **13**, 883 (1998).
63. H. Kishimoto, K. Takahama, N. Hashimoto, Y. Aoi, and S. Deki, *J. Mater. Chem.*, **8**, 2019 (1998).
64. K. Shimizu, H. Imai, H. Hirashima, and K. Tsukuma, *Thin Solid Films*, **351**, 220 (1999).
65. X.P. Wang, Y. Yu, X.F. Hu, and L. Gao, *Thin Solid Films*, **371**, 148 (2000).
66. M.K. Lee and B.H. Lei, *Jpn. J. Appl. Phys.*, **39**, L101 (2000).
67. T. Yao, I. Inui, and A. Ariyoshi, *J. Am. Ceram. Soc.*, **79**, 3329 (1996).
68. S. Deki, Y. Aoi, and A. Kajinami, *J. Mater. Sci.*, **32**, 4249 (1997).
69. S. Deki, Y. Aoi, Y. Miyake, A. Gotoh, and A. Kajinami, *Mater. Res. Bull.*, **31**, 1399 (1996).
70. S. Deki, Y. Aoi, J. Okibe, H. Yanagimoto, A. Kajinami, and M. Mizuhata, *J. Mater. Chem.*, **7**, 1769 (1997).
71. T. Yao, A. Ariyoshi, and T. Inui, *J. Am. Ceram. Soc.*, **80**, 2441 (1997).
72. T. Yao, *J. Mater. Res.*, **13**, 1091 (1998).
73. K. Tsukuma, T. Akiyama, and H. Imai, *J. Non-Cryst. Sol.*, **210**, 48 (1997).
74. W. Mindt, *J. Electrochem. Soc.*, **118**, 93 (1971).
75. T. Sasaki, Y. Matsumoto, J. Hombo, and M. Nagata, *J. Solid State Chem.*, **105**, 255 (1993).
76. M. Izaki and T. Omi, *J. Electrochem. Soc.*, **144**, L3 (1997).
77. M. Izaki and J. Katayama, *J. Electrochem. Soc.*, **147**, 210 (2000).
78. M. Izaki, *Electrochem. Solid State Lett.*, **1**, 215 (1998).
79. W. Mindt, *J. Electrochem. Soc.*, **117**, 615 (1970).
80. J. Emerson-Reynolds, *J. Chem. Soc.*, **45**, 162 (1884).
81. R.S. Mane and C.D. Lokhande, *Mater. Chem. Phys.*, **65**, 1 (2000).

82. L. Huang, P.K. Nair, M.T.S. Nair, R.A. Zingaro, and E.A. Meyers, *J. Electrochem. Soc.*, **141**, 2536 (1994).
83. P.K. Nair, L. Huang, M.T.S. Nair, H. Hu, E.A. Meyers, and R.A. Zingaro, *J. Mater. Res.*, **12**, 651 (1997).
84. S.G. Mokrushin and Y.D. Tkachev, *Colloid J. USSR*, **23**, 366 (1961).
85. G.A. Kitaev, S.G. Mokrushin, and A.A. Uritskaya, *Colloid J. USSR*, **27**, 38 (1965).
86. G.A. Kitaev, A.A. Uritskaya, and S.G. Mokrushin, *Russ. J. Phys. Chem.*, **39**, 1101 (1965).
87. G.A. Kitaev, A.A. Uritskaya, and S.G. Mokrushin, *Colloid J. USSR*, **27**, 317 (1965).
88. A.A. Uritskaya, G.A. Kitaev, and S.G. Mokrushin, *Colloid J. USSR*, **27**, 654 (1965).
89. G.A. Kitaev and A.A. Uritskaya, *Inorg. Mater.*, **2**, 1334 (1966).
90. G.A. Kitaev and T.S. Terekhova, *Russ. J. Inorg. Chem.*, **15**, 25 (1970).
91. G.M. Fofanov and G.A. Kitaev, *Russ. J. Inorg. Chem.*, **14**, 322 (1969).
92. N.D. Betenekov, V.P. Medvedev, and G.A. Kitaev, *Radiokhimiya*, **20**, 431 (1978).
93. N.D. Betenekov, V.P. Medvedev, A.S. Zhukovskaya, and G.A. Kitaev, *Radiokhimiya*, **20**, 608 (1978).
94. N.R. Pavaskar, C.A. Menezes, and A.P.B. Sinha, *J. Electrochem. Soc.*, **124**, 743 (1977).
95. I. Kaur, D.K. Pandya, and K.L. Chopra, *J. Electrochem. Soc.*, **127**, 943 (1980).
96. P.C. Rieke and S.B. Bentjen, *Chem. Mater.*, **5**, 43 (1993).
97. R.C. Kainthla, D.K. Pandya, and K.L. Chopra, *J. Electrochem. Soc.*, **127**, 277 (1980).
98. A. Lincot and R. Ortega-Borges, *J. Electrochem. Soc.*, **139**, 1880 (1992).
99. R. Ortega-Borges and D. Lincot, *J. Electrochem. Soc.*, **140**, 3464 (1993).
100. J.M. Doña and J. Herrero, *J. Electrochem. Soc.*, **139**, 2810 (1992).
101. J.M. Doña and J. Herrero, *J. Electrochem. Soc.*, **144**, 4081 (1997).
102. S. Gorer and G. Hodes, *J. Phys. Chem.*, **98**, 5338 (1994).
103. P. O'Brien and J. McAleese, *J. Mater. Chem.*, **8**, 2309 (1998).
104. P. O'Brien and T. Saeed, *J. Cryst. Growth*, **158**, 497 (1996).
105. M.L. Breen, J.T. Woodward, and D.K. Schwartz, *Chem. Mater.*, **10**, 710 (1998).
106. C.D. Lokhande, *Mater. Chem. Phys.*, **26**, 405 (1990).
107. D.S. Boyle, P. O'Brien, D. Otway, and O. Robbe, *J. Mater. Chem.*, **9**, 725 (1999).
108. D. Lincot, R. Ortega-Borges, and M. Froment, *Phil. Mag. B*, **68**, 185 (1993).
109. M. Froment and D. Lincot, *Electrochim. Acta*, **40**, 1293 (1995).
110. D. Lincot, R. Ortega-Borges, and M. Froment, *Appl. Phys. Lett.*, **64**, 569 (1994).
111. M. Froment, M.C. Bernard, R. Cortes, B. Mokili, and D. Lincot, *J. Electrochem. Soc.*, **142**, 2642 (1995).
112. H. Cachet, R. Cortes, M. Froment, G. Maurin, and N. Shramchenko, *J. Electrochem. Soc.*, **144**, 3583 (1997).
113. P.N. Gibson, M.E. Özsan, D. Lincot, P. Cowache, and D. Summa, *Thin Solid Films*, **361-362**, 34 (2000).
114. P.K. Nair, P. Parmananda, and M.T.S. Nair, *J. Cryst. Growth*, **206**, 68 (1999).
115. M. Kostoglou, N. Andritsos, and A.J. Karabelas, *Ind. Eng. Chem. Res.*, **39**, 3271 (2000).
116. E. Matijevic, *Ann. Rev. Mater. Sci.*, **15**, 483 (1985).
117. B.J. Tarasevich and P.C. Rieke, *Chem. Mater.*, **8**, 292 (1996).
118. F.C. Meldrum, J. Flath, and W. Knoll, *Langmuir*, **13**, 2033 (1997).
119. C.J. Milner and B.N. Watts, *Nature*, **163**, 322 (1949).
120. J.L. Davis and M.K. Norr, *J. Appl. Phys.*, **37**, 1670 (1966).
121. H. Sigmund and K. Berchthold, *Phys. Stat. Sol.*, **20**, 255 (1967).
122. P.K. Nair and M.T.S. Nair, *Solar Cells*, **22**, 103 (1987).
123. P.K. Nair, M.T.S. Nair, J. Campos, and L.E. Sansores, *Solar Cells*, **22**, 211 (1987).
124. R.W. Birkmire and E. Eser, *Ann. Rev. Mater. Sci.*, **27**, 625 (1997).
125. K. Durose, P.R. Edwards, and D.P. Halliway, *J. Cryst. Growth*, **197**, 733 (1999).
126. A.K. Turner, J.M. Woodcook, M.E. Özsan, D.W. Cunningham, D.R. Johnson, R.J. Marshall, N.B. Mason, S. Oktik, M.H. Patterson, S.J. Ransome, S. Roberts, M. Sadeghi, J.M. Sherborne, D. Sivapathsundaram, and I.A. Walls, *Solar Energy Mater. Solar Cells*, **35**, 263 (1994).
127. F.H. Karg, *Solar Energy Mater. Solar Cells*, **66**, 645 (2001).
128. M.T.S. Nair, P.K. Nair, R.A. Zingaro, and E.A. Meyers, *J. Appl. Phys.*, **75**, 1557 (1994).
129. T.L. Chu, S.S. Chu, C. Ferekides, C.Q. Wu, J. Britt, and C. Wang, *J. Appl. Phys.*, **70**, 7608 (1991).
130. T.L. Chu, S.S. Chu, N. Schultz, C. Wang, and C.Q. Wu, *J. Electrochem. Soc.*, **139**, 2443 (1992).
131. B.M. Basol and Y.K. Kapur, *IEEE Trans. Electron Devices*, **37**, 418 (1990).
132. Y. Hashimoto, N. Kohara, T. Negami, N. Nishitani, and T. Wada, *Solar Energy Mater. Solar Cells*, **50**, 71 (1998).
133. D. Braunger, D. Hariskos, T. Walter, and H.W. Schock, *Solar Energy Mater. Solar Cells*, **40**, 97 (1996).
134. K. Kushiya, M. Tachiyuki, T. Kase, I. Sugiyama, Y. Nagoya, D. Okumura, M. Sato, O. Yamase, and H. Takeshita, *Solar Energy Mater. Solar Cells*, **49**, 277 (1997).
135. A. Ennaoui, U. Blieske, and M.C. Lux-Steiner, *Prog. Photovolt. Res. Appl.*, **6**, 447 (1998).
136. C.D. Lokhande, A. Ennaoui, P.S. Patil, M. Giersig, K. Diesner, M. Muller, and H. Tribusch, *Thin Solid Films*, **340**, 18 (1999).
137. A. Ennaoui, *Can. J. Phys.*, **77**, 723 (1999).
138. A. Ennaoui, M. Weber, M. Saad, W. Harneit, M.C. Lux-Steiner, and F. Karg, *Thin Solid Films*, **361/362**, 450 (2000).
139. G. Contreras-Puente, O. Vigil, M. Ortega-López, A. Morales-Acevedo, J. Vidal, and M.L. Albor-Aguilera, *Thin Solid Films*, **361/362**, 378 (2000).
140. J. Herrero, M.T. Gutiérrez, C. Guillén, J.M. Doña, M.A. Martínez, A.M. Chaparro, and R. Bayón, *Thin Solid Films*, **361/362**, 28 (2000).
141. P.K. Vidyadharan-Pillai and K.P. Vijayakumar, *Solar Energy Mater. Solar Cells*, **51**, 47 (1998).
142. W.J. Danaher, L.E. Lyons, and G.C. Morris, *Solar Energy Mater.*, **12**, 137 (1985).
143. D.W. Niles, G. Herdt, and M. Al-Jassim, *J. Appl. Phys.*, **81**, 1978 (1997).
144. A. Kylner, J. Lindgren, and L. Stolt, *J. Electrochem. Soc.*, **143**, 2662 (1996).

145. A. Kylner, *J. Appl. Phys.*, **85**, 6858 (1999).
146. M. Weber, J. Krauser, A. Weidinger, J. Bruns, C.H. Fischer, W. Bohne, J. Röhrich, and R. Scheer, *J. Electrochem. Soc.*, **146**, 2131 (1999).
147. T. Nakada and A. Kunioka, *Appl. Phys. Lett.*, **74**, 2444 (1999).
148. T. Nakada, *Thin Solid Films*, **361/362**, 346 (2000).
149. L. Kronik, U. Rau, J.F. Guillemoles, D. Braunger, H.W. Schock, and D. Cahen, *Thin Solid Films*, **361/362**, 353 (2000).
150. R.G. Dhere, M.M. Al-Jassim, Y. Yan, K.M. Jones, H.R. Moutinho, T.A. Gessert, P. Sheldon, and L.L. Kazmerski, *J. Vac. Sci. Technol. A*, **18**, 1604 (2000).
151. A. Martel, F. Caballero-Briones, A.I. Oliva, R. Castro-Rodríguez, A. Iribarren, P. Bartolo-Pérez, and J.L. Peña, *Phys. Stat. Sol. B*, **220**, 261 (2000).
152. D.S. Boyle, S. Hearne, D.R. Johnson, and P. O'Brien, *J. Mater. Chem.*, **9**, 2879 (1999).
153. M.T.S. Nair and P.K. Nair, *Semicond. Sci. Technol.*, **4**, 191 (1989).
154. P.K. Nair, V.M. Garcia, A.M. Fernández, H.S. Ruiz, and M.T.S. Nair, *J. Phys. D Appl. Phys.*, **24**, 441 (1991).
155. P.K. Nair, M.T.S. Nair, O. Gomezdaza, and R.A. Zingaro, *J. Electrochem. Soc.*, **140**, 1085 (1993).
156. Y.F. Nicolau and J.C. Menard, *J. Appl. Electrochem.*, **20**, 1063 (1990).
157. V.P. Tolstoi, *Russ. Chem. Rev.*, **62**, 237 (1993).
158. Y.F. Nicolau, M. Dupuy, and M. Brunel, *J. Electrochem. Soc.*, **137**, 2915 (1990).
159. S. Lindroos, T. Kannianen, and M. Leskelä, *J. Mater. Chem.*, **6**, 1497 (1996).
160. M.P. Valkonen, S. Lindroos, and M. Leskelä, *Appl. Surf. Sci.*, **134**, 283 (1998).
161. G. Laukaitis, S. Lindroos, S. Tamulevičius, M. Leskelä, and M. Račkaitis, *Appl. Surf. Sci.*, **161**, 396 (2000).
162. S. Lindroos, T. Kanniainen, M. Leskelä, and E. Rauhala, *Thin Solid Films*, **263**, 79 (1995).
163. N.I. Kovtyukhova, E.V. Buzaneva, C.C. Waraksa, and T.E. Mallouk, *Mater. Sci. Eng. B*, **69/70**, 411 (2000).
164. R. Resch, G. Friedbacher, M. Grasserbauer, T. Kanniainen, S. Lindroos, M. Leskelä, and L. Niinistö, *Appl. Surf. Sci.*, **120**, 51 (1997).
165. T. Kanniainen, S. Lindroos, R. Resch, M. Leskelä, G. Friedbacher, and M. Grasserbauer, *Mater. Res. Bull.*, **35**, 1045 (2000).
166. M. Sasagawa, J. Nishino, and Y. Nosaka, *Electrochem.*, **67**, 1237 (1999).
167. Y.F. Nicolau and J.C. Menard, *J. Cryst. Growth*, **92**, 128 (1988).
168. V.V. Klechkovskaya, V.N. Maslov, M.B. Muradov, and S.A. Semiletov, *Sov. Phys. Crystallogr.*, **34**, 105 (1989).
169. R. Resch, T. Prohaska, G. Friedbacher, M. Grasserbauer, T. Kanniainen, S. Lindroos, M. Leskelä, L. Niinistö, and J.A.C. Broekaert, *Fresenius J. Anal. Chem.*, **353**, 772 (1995).
170. R. Resch, G. Friedbacher, M. Grasserbauer, T. Kanniainen, S. Lindroos, M. Leskelä, and L. Niinistö, *Fresenius J. Anal. Chem.*, **358**, 80 (1997).
171. T. Kanniainen, S. Lindroos, T. Prohaska, M. Leskelä, M. Grasserbauer, and L. Niinistö, *J. Mater. Chem.*, **5**, 985 (1995).
172. M.P. Valkonen, S. Lindroos, T. Kanniainen, M. Leskelä, R. Resch, G. Friedbacher, and M. Grasserbauer, *J. Mater. Res.*, **13**, 1688 (1998).
173. G. Laukaitis, S. Lindroos, S. Tamulevičius, M. Leskelä, and M. Račkaitis, *Mater. Sci. Eng. A*, **288**, 223 (2000).
174. M.P. Valkonen, S. Lindroos, R. Resch, M. Leskelä, G. Friedbacher, and M. Grasserbauer, *Appl. Surf. Sci.*, **136**, 131 (1998).
175. R. Resch, G. Friedbacher, M. Grasserbauer, S. Lindroos, T. Kanniainen, M.P. Valkonen, and M. Leskelä, *Fresenius J. Anal. Chem.*, **361**, 613 (1998).
176. S. Tamulevicius, M.P. Valkonen, G. Laukaitis, S. Lindroos, and M. Leskelä, *Thin Solid Films*, **355/356**, 430 (1999).
177. V.P. Tolstoi and E.V. Tolstobrov, *Inorg. Mater.*, **30**, 875 (1994).
178. E.V. Tolstobrov, V.P. Tolstoi, and I.V. Murin, *Inorg. Mater.*, **36**, 904 (2000).
179. H. Nagayama, H. Honda, and H. Kawahara, *J. Electrochem. Soc.*, **135**, 2013 (1988).
180. C.J. Huang, M.P. Houng, Y.H. Wang, N.F. Wang, and J.R. Chen, *J. Vac. Sci. Technol. A*, **16**, 2646 (1998).
181. J.S. Chou and S.C. Lee, *Appl. Phys. Lett.*, **64**, 1971 (1994).
182. J.S. Chou and S.C. Lee, *J. Electrochem. Soc.*, **141**, 3214 (1994).
183. C.F. Yeh, C.L. Chen, and G.H. Lin, *J. Electrochem. Soc.*, **141**, 3177 (1994).
184. T. Homma, T. Katoh, Y. Yamada, and Y. Murao, *J. Electrochem. Soc.*, **140**, 2410 (1993).
185. T. Homma and Y. Murao, *Thin Solid Films*, **249**, 15 (1994).
186. C.F. Yeh, S.S. Lin, T.Z. Yang, C.L. Chen, and Y.C. Wang, *IEEE Trans. Electron Devices*, **41**, 173 (1994).
187. C.F. Yeh and C.L. Chen, *Semicond. Sci. Technol.*, **9**, 1250 (1994).
188. C.F. Yeh, C.L. Chen, Y.C. Yang, S.S. Lin, T.Z. Yang, and T.Y. Hong, *Jpn. J. Appl. Phys.*, **33**, 1798 (1994).
189. A. Hishinuma, T. Goda, M. Kitaoka, S. Hayashi, and H. Kawahara, *Appl. Surf. Sci.*, **48/49**, 405 (1991).
190. J.H. Wei and S.C. Lee, *J. Electrochem. Soc.*, **144**, 1870 (1997).
191. M.K. Lee, C.N. Yang, C.H. Lin, and B.H. Lei, *Jpn. J. Appl. Phys.*, **37**, 423 (1998).
192. M.P. Houng, Y.H. Wang, N.F. Wang, C.J. Huang, and W.J. Chang, *Jpn. J. Appl. Phys.*, **36**, L696 (1997).
193. M.P. Houng, C.J. Huang, Y.H. Wang, N.F. Wang, and W.J. Chang, *J. Appl. Phys.*, **82**, 5788 (1997).
194. C.J. Huang, M.P. Houng, Y.H. Wang, and H.H. Wang, *J. Appl. Phys.*, **86**, 7151 (1999).
195. P. Chanthamaly, T. Arakawa, and N. Haneji, *Jpn. J. Appl. Phys.*, **38**, 5715 (1999).
196. C.F. Yeh and C.L. Chen, *J. Electrochem. Soc.*, **142**, 3579 (1995).
197. C.F. Yeh, S.S. Lin, and W. Lur, *J. Electrochem. Soc.*, **143**, 2658 (1996).
198. M.K. Lee, C.L. Yang, and C.H. Lin, *Jpn. J. Appl. Phys.*, **38**, 5048 (1999).
199. K. Awazu, H. Kawazoe, and K. Seki, *J. Non-Cryst. Solids*, **151**, 102 (1992).
200. C.F. Yeh, C.L. Chen, W. Lur, and P.W. Yen, *Appl. Phys. Lett.*, **66**, 938 (1995).
201. J.S. Chou and S.C. Lee, *IEEE Trans. Electron Devices*, **43**, 599 (1996).
202. W.S. Lu and J.G. Hwu, *Appl. Phys. Lett.*, **66**, 3322 (1995).
203. K.L. Yeh, M.J. Jeng, and J.G. Hwu, *Solid State Electr.*, **43**, 671 (1999).

204. C.F. Yeh and S.S. Lin, *J. Non-Cryst. Solids*, **187**, 81 (1995).
205. N.F. Wang, M.P. Houng, and Y.H. Wang, *Jpn. J. Appl. Phys.*, **38**, 5227 (1999).
206. H. Kawahara, Y. Sakai, T. Goda, A. Hishinuma, and K. Takemura, in *Glasses for Optoelectronics II*, edited by G.C. Righini (SPIE Proc. Series Vol. 1513, SPIE Press, Bellingham, 1991), pp. 198–203.
207. C.F. Yeh, Y.C. Lee, K.H. Wu, Y.C. Su, and S.C. Lee, *J. Electrochem. Soc.*, **147**, 330 (2000).
208. T. Horiuchi, K. Kanba, T. Homma, Y. Murao, and K. Okumura, *IEEE Trans. Electron Devices*, **40**, 1455 (1993).
209. C.F. Yeh, C.H. Liu, and J.L. Su, *J. Electrochem. Soc.*, **146**, 2294 (1999).
210. C.F. Yeh, T.Z. Yang, and T.J. Chen, *IEEE Trans. Electron Devices*, **42**, 307 (1995).
211. C.F. Yeh, T.J. Chen, and J.N. Jeng, *J. Electrochem. Soc.*, **144**, 3645 (1997).
212. M.S. Chen, J.S. Chou, and S.C. Lee, *IEEE Trans. Electron Devices*, **42**, 1918 (1995).
213. T. Homma, Y. Ariyama, H. Kondo, M. Sakamoto, S. Kanegae, M. Itoh, M. Yamaguchi, and H. Takahashi, *J. Electrochem. Soc.*, **147**, 1141 (2000).
214. K.C. Lee and J.G. Hwu, *IEEE Electron Devices Lett.*, **18**, 565 (1997).
215. K.C. Lee and J.G. Hwu, *J. Vac. Sci. Technol. A*, **16**, 2641 (1998).
216. F. Pearlstein, in *Encyclopedia of Materials Science and Engineering*, edited by M.B. Bever (Vol. 2, Pergamon Press, Oxford, 1986), pp. 1436–1440.
217. F. Goto, M. Ichimura, and E. Arai, *Jpn. J. Appl. Phys.*, **36**, L1146 (1997).
218. M. Ichimura, F. Goto, Y. Ono, and E. Arai, *J. Cryst. Growth*, **198/199**, 308 (1999).
219. M. Ichimura, F. Goto, and E. Arai, *J. Electrochem. Soc.*, **146**, 1028 (1999).
220. M. Ichimura, F. Goto, and E. Arai, *J. Appl. Phys.*, **85**, 7411 (1999).
221. P. Nemec, D. Mikes, J. Rohovec, E. Uhlírová, F. Trojánek, and P. Malý, *Mater. Sci. Eng. B*, **69/70**, 500 (2000).
222. C.T. Huang, P.H. Chang, and J.S. Shie, *J. Electrochem. Soc.*, **143**, 2044 (1996).
223. J.Y. Choi, K.J. Kim, J.B. Yoo, and D. Kim, *Solar Energy*, **64**, 41 (1998).
224. J.G. Vázques-Luna, R.B. López-Flores, M. Rubin-Falfán, L.D.C. Gómez-Pavón, R. Lozada-Morales, H. Juarez-Santiesteban, O. Starostenko, O. Zelaya-Angel, O. Vigil, O. Guzmán, P. delAngel, and A. Gónzalez, *J. Cryst. Growth*, **187**, 380 (1998).
225. O. Vigil, Y. Rodrìguez, O. Zelaya-Angel, C. Vàsquez-Lòpez, A. Morales-Acevedo, and J.G. Vàsquez-Luna, *Thin Solid Films*, **322**, 329 (1998).
226. J.G. Vázquez-Luna, A. Zehe, and O. Zelaya-Angel, *Cryst. Res. Technol.*, **34**, 949 (1999).
227. J.G. Vazques-Luna, A. Zehe, M.P. Trujillo-Garcia, and O. Starostenko, *Russ. J. Electrochem.*, **36**, 893 (2000).
228. M. Abe, *Electrochim. Acta*, **45**, 3337 (2000).
229. M. Abe, *MRS Bulletin*, **25**(9), 51 (2000).
230. M. Abe and Y. Tamaura, *Jpn. J. Appl. Phys.*, **22**, L511 (1983).
231. M. Abe and Y. Tamaura, *J. Appl. Phys.*, **55**, 2614 (1984).
232. M. Abe, Y. Tanno, and Y. Tamaura, *J. Appl. Phys.*, **57**, 3795 (1985).
233. Y. Goto, Y. Tamaura, M. Gomi, and M. Abe, *IEEE Transl. J. Magn. Jpn.*, **2**, 235 (1987).
234. Y. Goto, Y. Tamaura, M. Abe, and M. Gomi, *IEEE Transl. J. Magn. Jpn.*, **3**, 159 (1988).
235. M. Abe, T. Itoh, Y. Tamaura, Y. Goto, and M. Gomi, *IEEE Trans. Magnetics*, **MAG-23**, 3736 (1987).
236. J.S. Lee, T. Itoh, and M. Abe, *J. Korean Phys. Soc.*, **28**, 375 (1995).
237. T. Itoh, S. Hori, M. Abe, and Y. Tamaura, *Jpn. J. Appl. Phys.*, **29**, L1458 (1990).
238. T. Itoh, M. Abe, and Y. Tamaura, *J. Appl. Phys.*, **69**, 5911 (1991).
239. S. Hori, T. Itoh, M. Abe, and Y. Tamaura, *Jpn. J. Appl. Phys.*, **31**, 1185 (1992).
240. Q. Zhang, M. Gomi, T. Itoh, and M. Abe, *Jpn. J. Appl. Phys.*, **35**, L665 (1996).
241. T. Itoh, T. Miki, Q. Zhang, M. Abe, and Y. Tamaura, *Jpn. J. Appl. Phys.*, **34**, 1534 (1995).
242. M. Abe, *J. Phys. IV France*, **7**, 467 (1997).
243. Q. Zhang, T. Itoh, M. Abe, and M.J. Zhang, *J. Appl. Phys.*, **75**, 6094 (1994).
244. Y. Kitamoto, Y. Nakayama, and M. Abe, *J. Appl. Phys.*, **86**, 7130 (2000).
245. Y. Nakayama, H. Yajima, Y. Kitamoto, and M. Abe, *IEEE Trans. Magn.*, **35**, 3040 (1999).
246. M. Abe, Y. Kitamoto, K. Matsumoto, M.J. Zhang, and P.L. Li, *IEEE Trans. Magn.*, **33**, 3649 (1997).
247. K. Nishimura, Y. Kohara, Y. Kitamoto, and M. Abe, *J. Appl. Phys.*, **87**, 7127 (2000).
248. M. Abe, T. Miki, and Y. Kitamoto, *J. Phys. IV France*, **7**, 597 (1997).
249. M. Nagata and H. Iwahara, *Mater. Res. Bull.*, **28**, 255 (1993).
250. L. Addadi and S. Weiner, *Angew. Chem. Int. Ed.*, **31**, 153 (1992).
251. S. Mann, *J. Chem. Soc. Dalton Trans.*, **1997**, 3953 (1997).
252. P. Calvert and P. Rieke, *Chem. Mater.*, **8**, 1715 (1996).
253. S. Mann (Ed.), *Biomimetic Materials Chemistry* (VCH Publishers, Weinheim, 1996).
254. C.J. Brinker, *Curr. Op. Coll. Interf. Sci.*, **3**, 166 (1998).
255. P. Calvert and S. Mann, *J. Mater. Sci.*, **23**, 3801 (1988).
256. J. Sagiv, *J. Am. Chem. Soc.*, **102**, 92 (1980).
257. A. Ulman, *Chem. Rev.*, **96**, 1533 (1996).
258. P.C. Rieke, B.D. Marsh, L.L. Wood, B.J. Tarasevich, J. Liu, L. Song, and G.E. Fryxell, *Langmuir*, **11**, 318 (1995).
259. P.C. Rieke, R. Wiecek, B.D. Marsh, L.L. Wood, J. Liu, L. Song, G.E. Fryxell, and B.J. Tarasevich, *Langmuir*, **12**, 4266 (1996).
260. M. Maiti, R.J. Collins, U. Sampathkumaran, M.R. DeGuire, A.H. Heuer, and C.N. Sukenik, (unpublished work).
261. H. Shin, R.J. Collins, M.R. DeGuire, A.H. Heuer, and C.N. Sukenik, *J. Mater. Res.*, **10**, 692 (1995).
262. R.J. Collins, H. Shin, M.R. DeGuire, A.H. Heuer, and C.N. Sukenik, *Appl. Phys. Lett.*, **69**, 860 (1996).
263. H. Shin, M.R. DeGuire, and A.H. Heuer, *J. Appl. Phys.*, **83**, 3311 (1998).
264. T.P. Niesen, M.R. DeGuire, J. Bill, F. Aldinger, M. Rühle, A. Fischer, F.C. Jentoft, and R. Schlögl, *J. Mater. Res.*, **14**, 2464 (1999).
265. M. Agarwal, M.R. DeGuire, and A.H. Heuer, *J. Am. Ceram. Soc.*, **80**, 2967 (1997).

266. U. Sampathkumaran, M.R. DeGuire, A.H. Heuer, T. Niesen, J. Bill, and F. Aldinger, in *Innovative Processing and Synthesis of Ceramics, Glasses, and Composites II*, edited by N.P. Bansal and J.P. Singh (Ceramic Transactions Vol. 94, American Ceramic Society, Westerville, OH, 1999), pp. 307–318.
267. A. Fischer, F.C. Jentoft, G. Weinberg, R. Schlögl, T.P. Niesen, J. Bill, F. Aldinger, M.R. DeGuire, and M. Rühle, *J. Mater. Res.*, **14**, 3725 (1999).
268. M. Maiti, *Synthesis of Iron Oxide Thin Films on Organic Templates on Silicon*, M.S. Thesis, Case Western Reserve University, 1994.
269. Y. Wang, S. Supothina, M.R. DeGuire, A.H. Heuer, R. Collins, and C.N. Sukenik, *Chem. Mater.*, **10**, 2135 (1998).
270. S. Supothina, M.R. DeGuire, A.H. Heuer, T.P. Niesen, J. Bill, and F. Aldinger, in *Organic-Inorganic Hybrid Materials II*, edited by L.C. Klein, L.F. Francis, M.R. DeGuire, and J.E. Mark (MRS Symp. Proc. Vol. 576, Materials Research Society, Warrendale, PA, 1999), pp. 203–208.
271. S. Supothina and M. R. DeGuire, *Thin Solid Films*, **371**, 1 (2000).
272. U. Sampathkumaran, S. Supothina, R. Wang, and M.R. DeGuire, in *Mineralization in Natural and Synthetic Biominerals*, edited by P. Li, P. Calvert, R.J. Levy, T. Kokubo, and C.R. Scheid (MRS Symp. Proc., Vol. 599, Materials Research Society, Warrendale, PA, 2000), pp. 177–188.
273. M.R. DeGuire, T.P. Niesen, S. Supothina, J. Wolff, J. Bill, C.N. Sukenik, F. Aldinger, A.H. Heuer, and M. Rühle, *Z. Metallk.*, **89**, 758 (1998).
274. M. Agarwal, M.R. DeGuire, and A.H. Heuer, *Appl. Phys. Lett.*, **71**, 891 (1997).
275. H. Shin, M. Agarwal, M.R. DeGuire, and A.H. Heuer, *J. Am. Ceram. Soc.*, **79**, 1975 (1996).
276. T.P. Niesen, J. Wolff, J. Bill, M.R. DeGuire, and F. Aldinger, in *Organic-Inorganic Hybrid Materials II*, edited by L.C. Klein, L.F. Francis, M.R. DeGuire, and J.E. Mark (MRS Symp. Proc. Vol. 576, Materials Research Society, Warrendale, 1999), pp. 197–202.
277. J. Flath, F.C. Meldrum, and W. Knoll, *Thin Solid Films*, **327/329**, 506 (1998).
278. F. Meldrum, J. Flath, and W. Knoll, *J. Mater. Chem.*, **9**, 711 (1999).
279. F.C. Meldrum, J. Flath, and W. Knoll, *Thin Solid Films*, **348**, 188 (1999).
280. N.I. Kovtyukhova, E.V. Buzaneva, C.C. Waraksa, B.R. Martin, and T.E. Mallouk, *Chem. Mater.*, **12**, 383 (2000).
281. S. Baskaran, L. Song, J. Liu, Y.L. Chen, and G.L. Graff, *J. Am. Ceram. Soc.*, **81**, 401 (1998).
282. T.P. Niesen, J. Bill, and F. Aldinger, *Chem. Mater.* **13**(5) (2001).
283. H. Shin, M. Agarwal, M.R. DeGuire, and A.H. Heuer, *Acta Mater.*, **46**, 801 (1998).
284. M. Nagtegaal, P. Stroeve, and W. Tremel, *Thin Solid Films*, **327/329**, 571 (1998).
285. K.A. Ritley, K.P. Just, F. Schreiber, H. Dosch, T.P. Niesen, and F. Aldinger, *J. Mater. Res.*, **15**, 2706 (2000).
286. G.J. Kluth, M.M. Sung, and R. Maboudian, *Langmuir*, **13**, 3775 (1997).
287. P.C. Rieke, B.J. Tarasevich, L.L. Wood, M.H. Engelhard, D.R. Baer, G.E. Fryxell, C.M. John, D.A. Laken, and M.C. Jaehnig, *Langmuir*, **10**, 619 (1994).
288. B.C. Bunker, P.C. Rieke, B.J. Tarasevich, A.A. Campbell, G.E. Fryxell, G.L. Graff, L. Song, J. Liu, J.W. Virden, and G.L. McVay, *Science*, **264**, 48 (1994).
289. K. Koumoto, S. Seo, T. Sugiyama, and W.S. Seo, *Chem. Mater.*, **11**, 2305 (1999).
290. A. Kumar and G.M. Whitesides, *Appl. Phys. Lett.*, **63**, 2002 (1993).
291. S. Palacin, P.C. Hidber, J.P. Bourgoin, C. Miramond, C. Fermon, and G.M. Whitesides, *Chem. Mater.*, **8**, 1316 (1996).
292. Y.K. Hwang, S.Y. Woo, J.H. Lee, D.Y. Jung, and Y.U. Kwon, *Chem. Mater.*, **12**, 2059 (2000).
293. N.A. Kotov, I. Dekany, and J.H. Fendler, *J. Phys. Chem.*, **99**, 13065 (1995).
294. Y. Liu, A. Wang, and R. Claus, *J. Phys. Chem. B*, **101**, 1385 (1997).
295. I.A. Aksay, M. Trau, S. Manne, I. Honma, N. Yao, L. Zhou, P. Fenter, P.M. Eisenberger, and S.M. Gruner, *Science*, **273**, 892 (1996).
296. K. Ito and K. Shiraishi, *Solar Energy Mater. Solar Cells*, **35**, 179 (1994).
297. K. Ito and K. Tamaru, *J. Mater. Sci. Lett.*, **13**, 893 (1994).
298. I.O. Oladeji and L. Chow, *J. Electrochem. Soc.*, **144**, 2342 (1997).
299. I.O. Oladeji, L. Chow, J.R. Liu, W.K. Chu, A.N.P. Bustmante, C. Fredricksen, and A.F. Schulte, *Thin Solid Films*, **359**, 154 (2000).
300. D.S. Boyle, A. Bayer, M.R. Heinrich, O. Robbe, and P. O'Brien, *Thin Solid Films*, **361/362**, 150 (2000).
301. A. Bayer, D.S. Boyle, M.R. Heinrich, P. O'Brien, D.J. Otway, and O. Robbe, *Green Chem.*, **2**, 79 (2000).
302. K. Ito and K. Nakamura, *Thin Solid Films*, **286**, 35 (1996).
303. N.F. Wang, M.P. Houng, and Y.H. Wang, *Jpn. J. Appl. Phys.*, **38**, 6071 (1999).
304. M.K. Lee, B.L. Lei, and C.H. Lin, *Jpn. J. Appl. Phys.*, **36**, L979 (1997).
305. M. Abe, Y. Tamaura, Y. Goto, N. Kitamura, and M. Gomi, *J. Appl. Phys.*, **61**, 3211 (1987).
306. Q. Zhang, T. Itoh, and M. Abe, *J. Appl. Phys.*, **75**, 7171 (1994).
307. D. Huang, Z.D. Xiao, J.H. Gu, N.P. Huang, and C.W. Yuan, *Thin Solid Films*, **305**, 110 (1997).
308. Z. Xiao, J. Gu, D. Huang, Z. Lu, and Y. Wei, *Appl. Surf. Sci.*, **125**, 85 (1998).
309. Z. Xiao, L. Su, N. Gu, and Y. Wei, *Thin Solid Films*, **333**, 25 (1998).
310. Z. Xiao, M. Xu, J. Gu, D. Huang, and Z. Lu, *Mater. Chem. Phys.*, **52**, 170 (1998).
311. M. Nagtegaal, P. Stroeve, J. Ensling, P. Gütlich, M. Schurrer, H. Voit, J. Flath, J. Käshammer, W. Knoll, and W. Tremel, *Chem. Eur. J.*, **5**, 1331 (1999).